Drug crystal growth in ternary amorphous solid dispersions: Effect of surfactants and polymeric matrix-carriers

Afroditi Kapourani [a], Theodora Tzakri [a], Vasiliki Valkanioti [a],
Konstantinos N. Kontogiannopoulos [a,b], Panagiotis Barmpalexis [a,b,*]

[a] Department of Pharmaceutical Technology, School of Pharmacy, Aristotle University of Thessaloniki, Thessaloniki 54124, Greece
[b] Natural Products Research Centre of Excellence-AUTH (NatPro-AUTH), Center for Interdisciplinary Research and Innovation (CIRI-AUTH), Thessaloniki 57001, Greece

ARTICLE INFO

ABSTRACT

The present study evaluates the crystal growth rate of amorphous drugs when dispersed in different ternary polymeric amorphous solid dispersions (ASDs) in the presence of surfactants. Specifically, ternary ASDs of aprepitant (APT, selected as a model drug) were prepared via melt-quench cooling by evaluating three commonly used ASDs matrix/carriers, namely hydroxypropyl cellulose (HPC), poly(vinylpyrrolidone) (PVP) and the copolymer Soluplus® (SOL), and two suitable surfactants, namely d-alpha tocopheryl polyethylene glycol 1000 succinate (TPGS) and poly(ethylene glycol)-*block*-poly(propylene glycol)-*block*-poly(ethylene glycol) (P407). Results showed that all components were completely miscible (verified *via* hot stage polarized microscopy) and both surfactants were acting as plasticizers to the API. APT's crystal growth rate was increased in the presence of both P407 and TPGS, while PVP was identified as the matrix/carrier with the greatest impact API's crystal growth rate inhibition. Interestingly, TPGS presented a noticeable synergistic effect when combined with PVP resulting in a further reduction of APT's crystal growth rate. Furthermore, evaluation of APT's nucleation induction time in dissolution medium (PBS pH 6.8) revealed PVP as the most effective crystallization inhibitor, whereas the addition of TPGS showed to improve PVP's ability to inhibit APT's recrystallization. Finally, the formation of intermolecular interactions in the ternary APT-PVP-TPGS provided an explanation for the observed PVP-TPGS synergistic effects, with molecular dynamics simulations being able to unravel the type and extent of these interactions on a theoretical basis.

1. Introduction

It has been suggested that approximately 40% of currently marketed drugs and up to 75% of compounds under development in the pharmaceutical industry exhibit low aqueous solubility, leading to insufficient bioavailability (Janssens and Van den Mooter, 2009; Williams et al., 2013). Therefore, there is an urgent need for effective and affordable drug delivery strategies that will enhance drug solubility. Many techniques have been developed by the scientific community to overcome this challenge, among which, the preparation of amorphous solid dispersions (ASDs) has gained increased interest (Vasconcelos et al., 2007). Typically, an ASD consists of a single polymeric carrier in which an amorphous drug is molecularly dispersed, resulting in a single-phase amorphous mixture (Meng et al., 2017; Van den Mooter, 2012). Generally, there are high demands for an ASD system in order to be

regarded as successful. Specifically, it is critical for the prepared system to enhance the drug solubility and, at the same time, to stabilize the amorphous drug and prevent its recrystallization during processing or storage (Davis et al., 2018; Kyaw Oo et al., 2017a). Consequently, given that it is not possible for a single polymer to fulfil all requirements, an upsurge of research into ternary ASDs in the recent years is notable (Ghebremeskel et al., 2007; Kyaw Oo et al., 2017b; Nanaki et al., 2019; Prasad et al., 2014; Xie and Taylor, 2016).

In one specific group of ternary ASDs, which is getting increasing attention from both academic and industrial pharmaceutical formulation scientists, surface active compounds are being tested, such as surfactants, alone or in combination with suitable polymeric materials. These ternary systems seems to be effective in improving drug's dissolution and supersaturation characteristics (Goddeeris et al., 2008; Karataş et al., 2005; Lang et al., 2016; Meng et al., 2019; Moes et al.,

---

2011) although contracting results have also been reported (Chen et al., 2016). This improvement is achieved by reducing the interfacial energy barrier between the drug and dissolution medium, and hence improving the wettability, while API's solubility increases when the used surfactants are above their critical micelle concentration (CMC) (Chaudhari and Dugar, 2017; Gibaldi et al., 1968; Singh et al., 1968; Siriwannakij et al., 2021). Additionally, surfactants have been widely used as plasticizers in the ASDs prepared via hot-melt-extrusion (or other fusion-based techniques) (Fule and Amin, 2014; Fule et al., 2014; Ghebremeskel et al., 2007). In these cases, surfactants are incorporated in ASDs in order to facilitate the thermal processing and improve the thermomechanical properties of the prepared systems (Chaudhari and Dugar, 2017). However, despite the wide attention paid for the preparation of surfactant-based ternary ASDs (and the focus on their advantages regarding API's dissolution rate enhancement and plasticizing ability) there are still several aspects that need further evaluation (such as drug's physical stability and recrystallization tendency during storage and dissolution) before adopting them as an efficient amorphous pharmaceutical formulation technique.

As far as the effect of the surfactants on APIs' physical stability during storage is concerned, a previously published study has shown the significant impact of three commonly used surfactants (i.e., sodium lauryl sulfate, sucrose palmitate and D-α-Tocopheryl polyethylene glycol 1000 succinate) on the crystal growth of celecoxib, both in the presence and absence of a polymer (i.e. poly(vinylpyrrolidone), PVP) (Mosquera-Giraldo et al., 2014). This study revealed that the crystallization rate of celecoxib was increased in the presence of surfactants, and hence the selection of a proper surfactant for a ternary ASD is a nontrivial procedure. However, other reports, also evaluating the impact of surfactants on drug's re-crystallization tendency, have shown contradictory results (Chaudhari and Dugar, 2017; Feng et al., 2018; Kojima et al., 2012; Ueda et al., 2017; Wang et al., 2005).

In regard to surfactants' effect on APIs' recrystallization during supersaturation studies, Chen et al. and Zhang et al. have both reported that, depending on their type, surfactants may either increase or decrease API's nucleating time and rate of desaturation during dissolution (Chen et al., 2015; Zhang et al., 2019), while other studies showed that the use of surfactants destabilizes API's supersaturation maintenance (Chen et al., 2016; Deshpande et al., 2018; Liu et al., 2016). Furthermore, Ueda et al. have recently reported that the presence of a surfactant alone did not effectively suppress coarsening of the ketoprofen - rich phase generated by liquid-liquid phase separation, while a combined use of a surfactant with hydroxypropyl methylcellulose (HPMC) resulted in a smaller size of the ketoprofen - rich droplet, as compared to HPMC solutions without surfactants (Ueda and Taylor, 2021). Therefore, these recent published attempts, although limited in number, indicate that a comprehensive evaluation on the effect of surfactant-induced API re-crystallization in ASDs is of crucial importance.

In this context, the present study is attempting to gain a further insight into the field, by extending the work of other research groups in regard to surfactant-based ternary ASDs characterization. For this purpose, ternary ASDs were prepared via melt mixing approach, using aprepitant (APT, an antiemetic agent having P/neurokinin 1 (NK1) receptors antagonist properties (Barmpalexis et al., 2018a)) as a poor water soluble model drug, along with three commonly used polymeric matrix-carriers (namely, hydroxypropyl cellulose, HPC-SL, povidone, PVP, and polyvinyl caprolactam–polyvinyl acetate–polyethylene glycol graft copolymer, Soluplus®) (Barmpalexis et al., 2018b; Barmpalexis et al., 2019; Ben Osman et al., 2018; Kapourani et al., 2020b) and two widely used pharmaceutical surfactants (i.e., d-alpha tocopheryl polyethylene glycol 1000 succinate, TPGS, and poly(ethylene glycol)-*block*-poly(propylene glycol)-*block*-poly(ethylene glycol), Poloxamer 407). The prepared systems were evaluated in terms of API's crystal growth rate, water-induced nucleation induction time, amorphous suspension stability and molecular interactions both experimentally and

theoretically (via molecular dynamics, MD, simulations).

2. Material and methods

2.1. Materials

APT (mixture of form I and II, Jubilant Generics Limited, Karnataka, India) was kindly given as a gift from Rontis Hellas S.A. (Athens, Greece). Graft copolymer Soluplus® (SOL), PVP (Kollidon®K12), TPGS (Kolliphor®TPGS, TPGS) and Poloxamer 407 (P407, Kolliphor® 407) were obtained from BASF (Ludwigshafen, Germany). HPC-SL was obtained from Shin-Etsu (Nigata, Japan). All other reagents were of analytical or pharmaceutical grade and used as received.

2.2. Preparation of ASDs

Preparation of all amorphous samples and ASDs was conducted via melt / quench-cooling. Specifically, suitable amounts of pure APT, APT-matrix/carrier or APT-surfactant-matrix/carrier systems (~ 1 g of total weight, at various weight ratios) were placed in appropriate aluminum pans and melted at 260 °C on a heating plate under N_2 in order to avoid any degradation induced by oxidation. The melted samples were then rapidly solidified by quench-cooling at −8 °C in a freezer. The obtained amorphous dispersions were ground gently using a mortar and pestle, and then sieved to obtain a size range of 150–180 μm. Polarized light microscopy (PLM) and differential scanning calorimetry (DSC) were used in order to verify that the API remained amorphous after grinding and sieving. All samples were stored in glass containers closed hermetically (rubber stopper reinforced with an Apiezon Q seal) and placed in zero-humidity desiccants (P_2O_5) before further use.

Thermogravimetric analysis (TGA, Shimadzu TGA-50 thermogravimetric analyzer, Tokyo, Japan) was employed in order to evaluate components' thermal stability during ASD preparation process. For the analysis approximately 10.0 mg of samples were placed into suitable aluminum sample pans, attached to a sensitive microbalance assembly, and heated from 30 to 300 °C at a rate of 10 °C/min, using nitrogen as purge gas at a flow rate of 25 mL/min. The weight variation of the samples was recorded in relation to temperature, while all experiments were conducted in triplicate.

2.3. Miscibility evaluation

Hot stage polarized microscopy (HSM) was used for the experimental evaluation of component's miscibility. Specifically, physical mixtures of: i) APT with surfactants at a ratio of 10/90 *w*/w of API to surfactant, ii) APT with matrix/carriers at a ratio of 10/90 w/w of API to matrix/carrier and iii) APT with surfactants and matrix/carriers at a ratio of 10/10/80 w/w of APT to surfactant to matrix/carrier were heated from 25 °C until complete melting (at a rate of 10 °C/min), on a Linkam THMS600 heating stage (Linkam Scientific Instruments Ltd., Surrey, UK), mounted on Olympus BX41 polarized light microscope, and controlled through a Linkam TP94 temperature controller. Evaluation of miscibility was made by visual observation.

2.4. Crystal growth rate measurements

The effect of surfactants and polymeric matrix/carriers on APT's crystal growth was evaluated via polarized light microscopy (Olympus BX41 polarized light microscope, Olympus, Tokyo, Japan) according to a previously published methodology (Mosquera-Giraldo et al., 2014). In brief, physical mixtures of APT and surfactants or matrix/carriers at a ratio of 90/10 w/w of API to surfactant or matrix/carrier were mixed with a mortar and pestle for 5 min in order to obtain a homogenous blend. Similarly, ternary physical mixtures of APT (80 wt%), matrix/carrier (10 wt%) and surfactant (10 wt%) were also prepared. Afterwards, 3–5 mg of each mixture, were placed on a suitable microscopy

slide with a cover slip and heated (with a rate of 10 °C/min) just above APT's melting temperature into a Linkam THMS600 heating stage (Linkam Scientific Instruments Ltd., Surrey, UK), mounted on Olympus BX41 polarized light microscope, and controlled through a Linkam TP94 temperature controller. Then, the samples were quenched-cooled to room temperature in order to obtain an ASD. Subsequently, the obtained amorphous samples were seeded with APT crystals at the edge of the cover slip and the growth rate of the APT crystal interface was monitored at temperatures over the range of 180–220 °C, by taking time lapse pictures. This temperature range was selected based on APT's recrystallization pattern after a heat-cool-heat cycle in 204 F1 Phoenix heat flux (NETZSCH, Germany) differential scanning calorimeter (DSC). In all cases, the growth rates were determined in triplicate at each temperature from the slope of the linear plot of the crystal front advancement vs. time.

2.5. Differential scanning calorimetry (DSC)

In order to evaluate the effect of the selected surfactants, matrix/carriers and surfactants-matrix/carrier systems on the melting point (T_m) and glass transition temperature (T_g) of APT, DSC measurements were performed in a DSC 204 F1 Phoenix heat flux (NETZSCH, Germany). Specifically, samples (~ 5.0 mg) were melt-quenched in a DSC 204 F1 Phoenix heat flux DSC (NETZSCH, Germany), by heating to 10 °C above the melting point of APT with a heating rate of 10 °C/min, keeping it isothermal for 3 min, in order to erase any thermal history, cooling at a rate of 10 °C/min to approximately 30 °C, before re-heating again at the same rate, up to 260 °C. APT's melting point was determined as the onset temperature of the heat flow curve ($T_{melt,ons}$), T_g was determined as the inflection point temperature, while enthalpy of fusion (ΔH_f) was determined as the integrated area of the heat flow curve in all cases. The standard deviations of temperatures and enthalpies determined in this work were not higher than 1.0 °C and 3.0 J/g, respectively. Nitrogen flow (50 mL/min) was applied in order to provide a constant thermal blanket within the DSC cell. The instrument was calibrated for temperature using high purity benzophenone, indium, and tin, while the enthalpic response was calibrated using indium. Thermograms were analyzed using the NETZSCH Proteus – Thermal Analysis software package version 5.2.1 (NETZSCH, Germany). All experiments were conducted in triplicate.

2.6. Powder X-ray diffracrometry (pXRD)

pXRD patterns of the pure components, APT-surfactants, APT-matrix/carrier or APT-surfactant-matrix/carrier systems ASDs (prepared according to Section 2.2) were recorded using an X-ray diffractometer (Rigaku - Miniflex II) with a CuKα radiation source for crystalline phase identification ($\lambda = 0.15405$ nm for CuKα) immediately after preparation. All samples were scanned from 5 to 40°.

2.7. Determination of critical micelle concentration (CMC)

Since the presence of drug molecules affect the CMC of surfactants, in the present study the CMC of the tested surfactants was evaluated by measuring the solubility of APT in solutions containing varying amounts of them. Specifically, excess amount of crystalline APT was equilibrated in aqueous media, with different surfactant concentrations for 48 h at 37 °C. After equilibration, the samples were removed and filtrated with 0.1 μm PVDF filters and analyzed via a validated high-performance liquid chromatography method. Specifically, a Shimadzu HPLC system consisting of a LC-10 CE VP pump, an autosampler model SIL-20A HT equipped with a 100 μL loop and a UV–vis detector model SPD-10A VP (Tokyo, Japan) was used. Class VP Chromatography data system version 4.3 was the software used. UV detector was set at 210 nm, while Ascentics C8 (15cm × 4.6 mm, 5 μm) was used as a column. The mobile phase consisted of ACN: H_3PO_4 (0.1% w/v) in a ratio of 60:40 v/v, with a

1.0 mL/min flow rate. For the determination of the drug content 30 μL were used as injection volume with a runtime of 8 min. The calibration curves for APT were linear ($R^2 > 0.999$) in the range of 1–12 μg/mL. All measurements were conducted in triplicate and the surfactants' CMC was determined at the concentration where an abrupt increase of APT solubility was observed.

2.8. Nucleation induction time studies

Surfactants' and matrix/carriers' effect on the crystallization tendency of APT within a supersaturated solution was evaluated by measuring the nucleation induction time using a method described previously (Chen et al., 2015; Ilevbare and Taylor, 2013). Briefly, in order to achieve supersaturation, solubilized APT in methanol (4 mg/mL) was titrated into 80 mL of a buffered solution at pH 6.8 equilibrated at 37 °C. High agitation speed (i.e., 300 rpm) was achieved via a cross-shaped magnetic stirrer. The onset of nucleation was determined from the increase in intensity of light scattered from the drug solutions upon evolution of particles, measured at 380 nm using a SI Photonics UV/vis spectrometer (Tuscon, Arizona) fiber, optically coupled with a dip probe (path-length 10 mm). Since APT has no absorbance in this wavelength, the turbidity was the only contributor to the changed absorbance. APT's solution concentration was also monitored at 210 nm for verification. The experiments were conducted in the absence and presence of pre-dissolved surfactants (at 11% above CMC) and matrix/carriers (at a concentration of 5 μg/mL). All studies were performed in constant initial supersaturation conditions five times the equilibrium concentration of the crystalline APT measured in the presence of each pre-dissolved additive compound ($S = 5$), in order to ensure a constant nucleation driving force among all studied systems. Additionally, the same measurements were also conducted at a lower degree of supersaturation ($S = 2.5$) in order to check the role of supersaturation in API's nucleation induction time. All experiments were conducted in triplicate.

2.9. Amorphous suspension stability and re-crystallization studies

APT physical stability within the amorphous suspension system was assessed by adding 100 mg of APT-matrix/carrier ASDs (at a 30/70% w/w API to matrix/carrier ratio) into 10 mL of aqueous buffer solution at pH 6.8 (PBS). Three different liquid media were tested, namely PBS with and without surfactants (P407 and TPGS). All surfactant concentrations were 11% above the previously estimated CMC. A drop of the suspension was placed on a microscope slide and visually inspected under a PLM at time intervals of 0.5, 1, 2, 4, 6, 24 and 48 h, where the stability of the amorphous suspension was assessed based on the presence or absence of crystalline birefringent particles. All experiments were conducted in triplicate.

2.10. Molecular interactions

2.10.1. ATR-FTIR spectroscopy

Possible molecular interactions evolving within the ASDs were experimentally evaluated via ATR-FTIR spectroscopy. Specifically, for the collection of the ATR-FTIR spectra of the raw materials and the samples (containing 90/10 wt% of API to matrix/carrier, in the case of binary ASDs, and 80/10/10 wt% of API to matrix/carrier to surfactant, in the case of ternary ASDs) a small quantity of each sample (~15 mg) were placed on the ATR crystal top plate of a Golden Gate™ MKII Single Reflection Diamond ATR System (Specac, Kent, UK) mounted into Shimadzu IR-Prestige-21 FT-IR infrared spectrometer (Tokyo, Japan) with Benchmark™ baseplate. The angular incidence of light at the ATR crystal sample interface was 45°, while the beam condensing lenses used in the optical unit were made of ZnSe with an anti-reflection coating, and the anvil used was made from sapphire. A 1.66 μm at 1000 cm^{-1} depth of penetration, a 2.4 refractive index and a 525 cm^{-1} long wavelength cut-off were set for the ATR system. The samples were
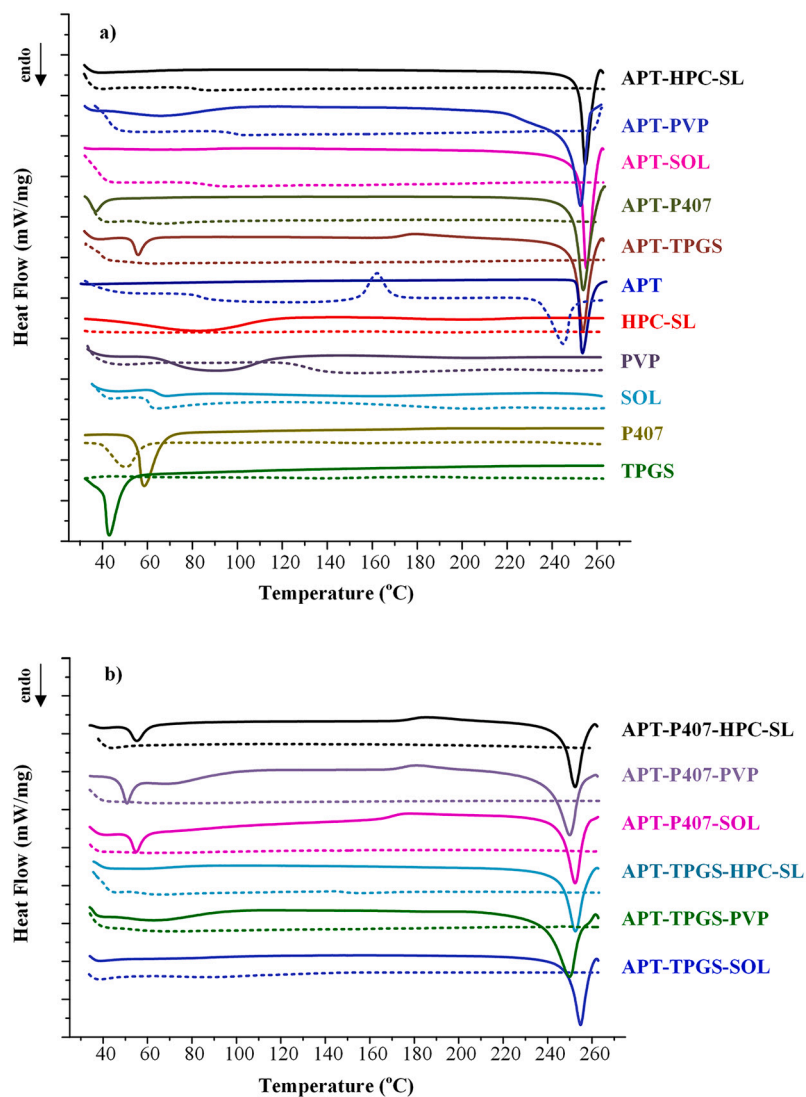
Fig. 1. DSC thermograms of: a) raw materials and binary physical mixtures; and b) ternary systems (1st heating scans are given with solid-lines while 2nd heating scan is given with dashed-lines).

scanned in the region of 4000–750 cm^{-1} after appropriate background subtraction and sixty-four (64) scans over the selected wavenumber range were collected (at a resolution of 4 cm^{-1}) and averaged for each sample using the IRsolution 1.30 software program (Shimadzu, Tokyo, Japan). In addition to the ASD samples analyzed immediately after preparation, the changes in the molecular interactions occurring during their hydration/solubilization process were evaluated by exposing them to the dissolution medium for a few minutes (~5 min), and then (after wiping away excess water from the surface with filter paper), analyzing with ATR-FTIR using the same instrument and methodology described previously.

2.10.2. Molecular dynamics (MD) simulation

In addition to ATR-FTIR, molecular interactions were also evaluated on a theoretical basis via MD simulations. In brief, the initial structures of the API and the rest components (corresponding to the most promising ternary ASD system) were prepared using VEGAZZ v.3.1.2.39 (Pedretti et al., 2004) and then, optimized via energy minimization using the *pcff_d* force field (Sun et al., 1994). All MD simulations were performed with the XenoView v.3.7.9.0 molecular simulation suite free available on-line (http://www.vemmer.org/xenoview/xenoview.html). A total of ten structures (for each component) were optimized and those with the lowest energy were selected for further analysis. In a further

step, amorphous cells of the initially optimized components were prepared using Xenoview's amorphous builder, by varying the rotatable torsions via the free rotation model method. A total of ten independent simulation boxes were constructed and subjected to geometry optimization runs using the steepest descent algorithm in order to remove any unfavorable interactions and attain the lowest energy state. During the actual MD simulation runs an equilibration phase was initially employed in order to relax the obtained structures for 2.0 ns under the NVT at 260 °C (approximately the temperature used for the preparation of ASDs) with *pcff_d* force field, 1.0 fs time step and Berendsen thermostat. Then, the structures obtained were subjected in a further 1.0 ns processing under NPT (variable volume and shape) at atmospheric pressure (1 atm) and 260 °C, using the same force field, a cut-off radius of 10.0 Å, spline distance of 1 Å, Berendsen thermostat & barostat, and 1.0 fs time step. In all cases, the validity of the simulations was ensured by following the criteria suggested by van Gunsteren and Mark (Gunsteren and Mark, 1998).

In addition, MD simulations were also conducted in the presence of water in order to evaluate for changes occurring in systems' molecular interactions during their hydration/solubilization process. In this case the same MD procedure, as the one described above, was followed for the preparation of initial conformations, with the addition of 200 water molecules surrounding the prepared structures. For the preparation of
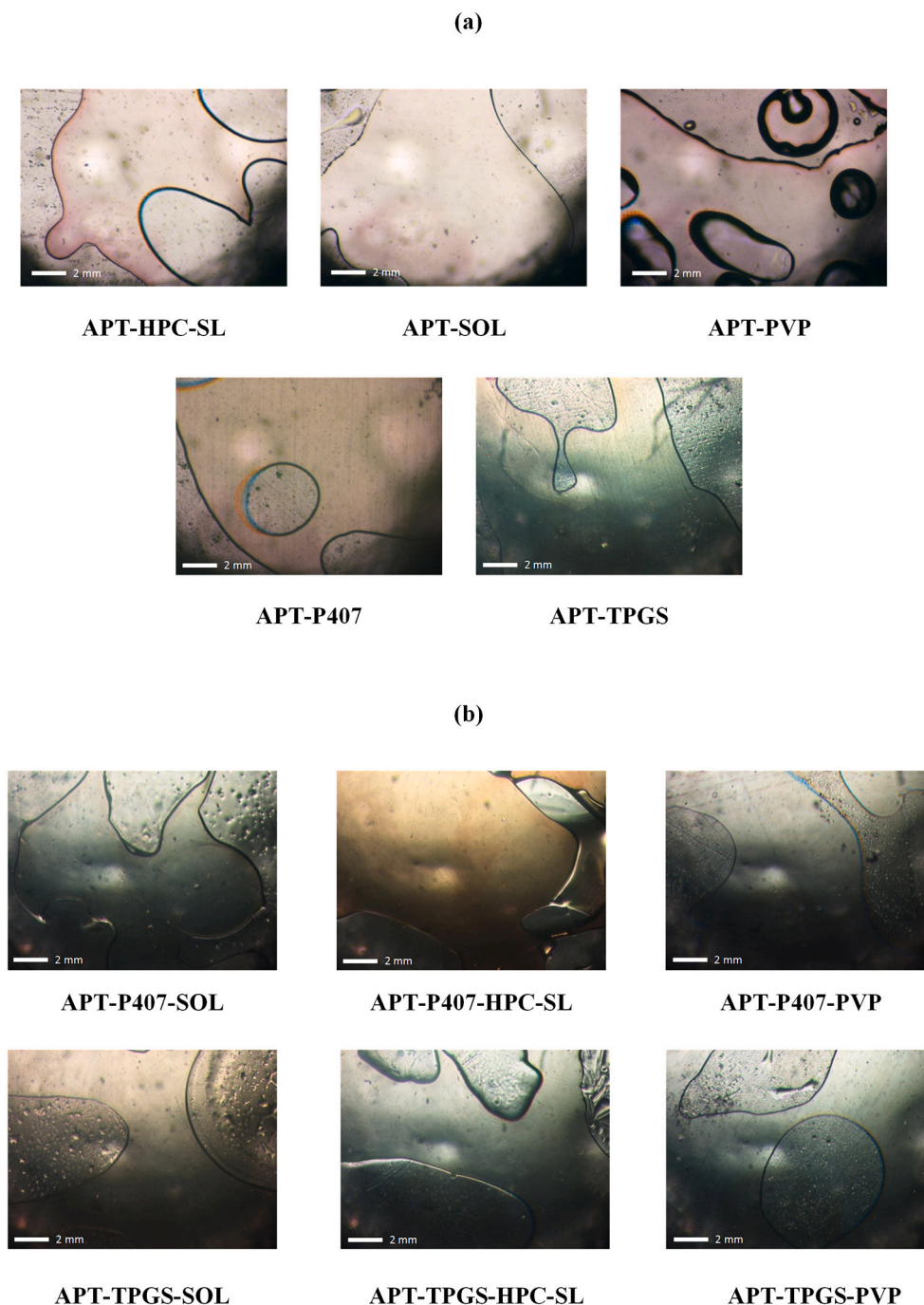
(a)

APT-HPC-SL   APT-SOL   APT-PVP

APT-P407   APT-TPGS

(b)

APT-P407-SOL   APT-P407-HPC-SL   APT-P407-PVP

APT-TPGS-SOL   APT-TPGS-HPC-SL   APT-TPGS-PVP

Fig. 2. HSM photographs for the melting process of binary mixtures at: a) 10/90 w/w APT to matrix-carrier/surfactant ratio, and b) ternary mixtures at a 10/10/80 *w*/w APT to matrix-carrier to surfactant ratio.

water molecules, the TIP3P (transferable intermolecular potential 3P) model was used (i.e., O–H length was set at 0.9572 Å, H–O–H angle at 104.52^o, and oxygen and hydrogen point charges at −0.834 and + 0.417, respectively) and the obtained amorphous cells were subjected to MD simulation runs at 37 °C for a total of 3.0 ns (0.0 ns NVT for equilibration and 1.0 ns NPT for data collection).

3. Results and discussion

3.1. Thermal stability results

Initially, for the preparation of any ASD system via a melt-based approach (such as melt mixing, hot-melt extrusion etc.) it is important

to ensure that the applied melting temperature does not lead to any thermal degradation phenomena. Hence, in order to evaluate the thermal degradation profile of all used components and ensure their thermal stability during the ASD preparation, TGA was performed. According to the obtained results (Fig. S1, supplementary material), APT was thermally stable up to approximately 268 °C, with no traces of moisture, while PVP showed a noticeable weight loss (~7.0% *w*/w) at temperatures below 100 °C, attributed to the presence of free water. In the case of SOL, an initial mass loss (~3.0%) was recorded up to 130.0 °C, due to the presence of residual moisture water, followed by a second mass loss phase (starting from approximately 275.0 °C), while HPC-SL showed only the presence of a small percentage of residual moisture-water (~1.3%). In the case of P407, the obtained TGA thermogram did not
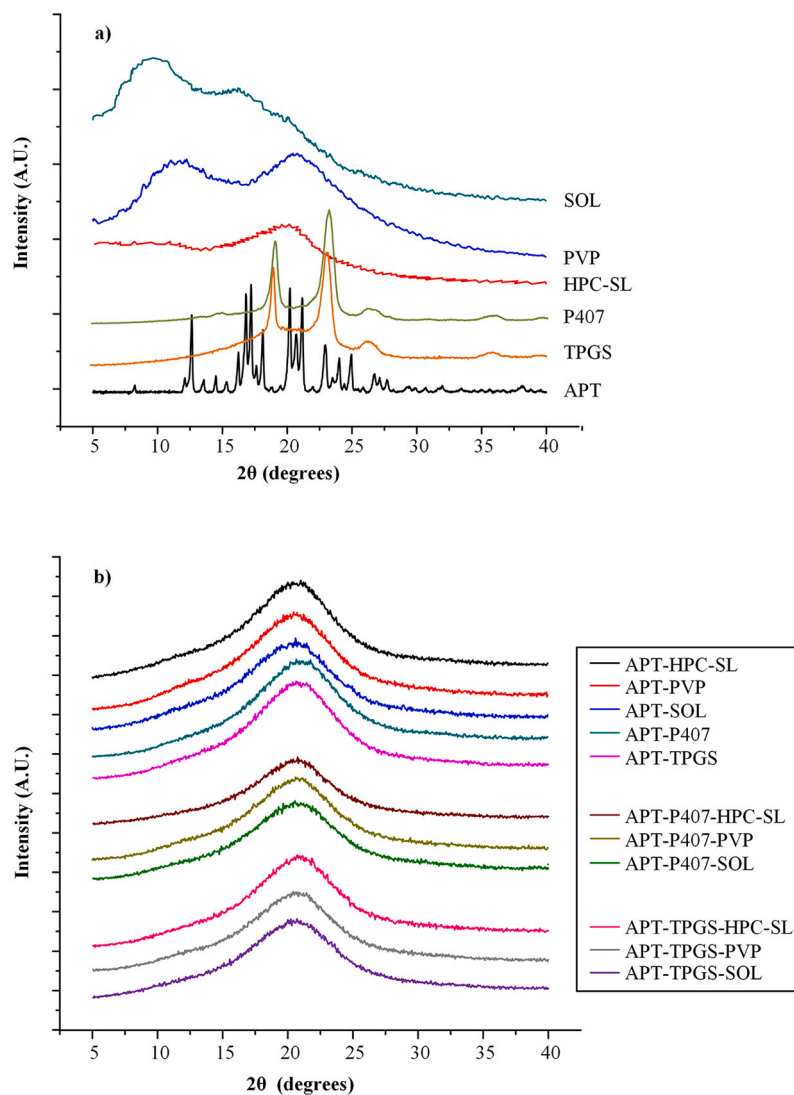
Fig. 3. Powder X-ray diffractograms for the raw materials (a) and prepared binary and ternary APT ASDs (b).

show any residual water, while a mass loss (i.e., thermal degradation) phase was recorded starting at approximately 270.0 °C. Finally, TGA thermograms for TPGS did not show any sample weight losses up to 300 °C. Hence, based on the obtained thermograms, all components were thermally stable up to 260 °C, ensuring thus their safe thermal processing during the preparation of APT ASDs.

3.2. Analysis of ASD's thermal properties

Following TGA, DSC was performed in order to evaluate the thermal properties of the prepared ASD systems (Fig. 1). In respect to the pure API, results from the 1st heating scan in Fig. 1a showed a melting endotherm at $T_{melt,ons} = 251.42$ °C (ΔH_f of 118.56 J/g) corresponding to the co-melting of APT form I and II crystals, while upon reheating the API showed a single T_g at 84.10 °C, followed by a recrystallization exotherm at 145.83 °C and a melting endotherm at $T_{melt,ons}$ of 237.38 °C. Based on this thermal profile the API can be considered as a non-stable glass former (this is in agreement with previously published results (Kapourani et al., 2020b)). In the case of HPC-SL a broad endothermic peak was recorded during the 1st DSC heating scan, corresponding to the presence of residual moisture, while 2nd DSC heating scans for PVP and SOL showed a T_g at 138.15 °C and 65.26 °C, respectively. Finally, in respect to the raw materials the DSC thermograms for P407 and TPGS revealed a single endothermic melting peak at $T_{melt,ons}$ of 54.20 °C (ΔH_f

= 111.13 J/g), and 39.19 °C ($\Delta H_f = 114.51$ J/g), respectively.

In regard to APT-polymer binary mixtures, results for APT-HPC-SL in Fig. 1a showed a single endothermic peak at $T_{melt, ons} = 251.67$ °C ($\Delta H_f = 82.79$ J/g), corresponding to the melting of APT, while the 2nd heating run revealed a single T_g at 81.39 °C. Similarly, in the case of binary APT-PVP, a DSC endotherm was recorded at $T_{melt, ons} = 248.38$ °C ($\Delta H_f = 101.52$ J/g) corresponding to the melting of the API, while, upon reheating, a single T_g was recorded at 92.89 °C. Also, results on APT-SOL showed APT's melting peak ($T_{melt,ons}$) at 251.83 °C (with a ΔH_f of 84.00 J/g) in the 1st heating run, while a single T_g was recorded upon reheating at 86.08 °C. In regard to API-surfactant binary systems, the DSC thermograms of APT-TPGS revealed one small endothermic peak at $T_{melt,ons} = 33.27$ °C ($\Delta H_f = 11.91$ J/g), corresponding to the melting of neat TPGS, followed by a second endothermic peak at $T_{melt, ons} = 249.73$ °C ($\Delta H_f = 86.00$ J/g), due to the melting of the crystalline API, while upon reheating of the binary system showed a single T_g at 57.42 °C. Similarly, in the case of APT-P407 system, two endothermic peaks are recorded during the 1st heating scan of the sample. The first, recorded at $T_{melt, ons} = 52.83$ °C ($\Delta H_f = 10.50$ J/g), was related to the melting of P407, while the second ($T_{melt, ons} = 249.86$ °C with ΔH_f of 87.25 J/g), was attributed to APT's melting. As in the case of APT-TPGS, during the DSC reheating of the APT-P407 sample, a single T_g was also recorded (at 53.67 °C).

It should be noted that according to the obtained DSC results for the

binary mixtures, APT seems to be less effectively dispersed (dissolved) within the PVP melt (since a higher ΔH_f value was recorded as compared to the rest carriers), while in all cases a single T_g was recorded after the DSC in-situ melt – quench cooling, indicating that all tested polymers and surfactants were probably miscible with the API. However, although APT-PVP melts seemed to be less favorable, the use of PVP, as compared to the rest binary components, lead to a higher single ASD T_g value, indicating enhanced anti-plasticizing effect on the API. In addition, taking into consideration that the glass transition temperature of APT is 84.10 °C (a similar T_g was also reported previously (Kapourani et al., 2020b)), both surfactants (i.e., P407 and TPGS) showed a significant plasticizing ability. Moreover, based on the obtained DSC thermograms it should be noted that no API melting endotherms were recorded upon samples' reheating (i.e., 2nd DSC heating runs), indicating that the API was probably amorphously dispersed within all binary systems.

Finally, in the case of APT-polymer-surfactant ternary mixtures, results in Fig. 1b showed that both surfactants acted as plasticizers, since the melting point of the API was further reduced in all cases (as compared to the respective binary mixtures). Additionally, upon reheating one single T_g was observed in all samples, while no APT melting endotherms were recorded, indicating that a complete amorphization of the API was probably also achieved in all ternary systems (ASD physical state is also evaluated in Section 3.4).

3.3. Component's miscibility evaluation

The components' miscibility, during the preparation of an ASD, is profoundly related to the physical stability of the system (Qian et al., 2010; Solanki et al., 2019). Immiscibility and mutual incompatibility may result to phase separation and, subsequently, to higher recrystallization tendency for the API (Ma and Williams, 2019). Nevertheless, a well-established method does not yet exist to adequately predict whether the ASD's components are miscible (Qian et al., 2010). Although the most frequently used method is the identification of a single T_g using DSC, recent studies have proved that this approach possesses several drawbacks (Yuan et al., 2014). Consequently, several other techniques are currently being utilized for the evaluation of miscibility. These include pXRD, solid-state NMR and HSM, the latter of which is considered as the easiest to implement (Kapourani et al., 2019; Newman et al., 2008; Pham et al., 2010). With HSM, miscibility in the melt state can be easily detected, since miscible compounds form a uniform liquid melt. Fig. 2 presents the obtained HSM images at the melting point of the binary and ternary APT samples. In all cases, no API crystals were observed, indicating that APT is either melted, or dispersed in amorphous state, within the evaluated systems during the preparation of ASDs. Additionally, based on the obtained results, APT and all components, were completely miscible at the melt state, since no de-mixing zones were observed between them, a strong indication of good miscibility between all ASD's components.

3.4. ASD's physical state evaluation

APT's physical state in the prepared ASDs (both binary and ternary mixtures) was evaluated via pXRD. Fig. 3a shows the pXRD diffractograms of all raw materials. APT's diffractogram revealed the crystalline nature of the neat API. Specifically, several characteristic diffraction peaks were recorded at $2\theta = 8.2, 12.6, 16.2, 16.8, 17.2, 18.1, 20.2, 20.7, 21.2, 22.9, 24.0$ and $24.9°$, indicating that the API was a mixture of polymorphs I and II. As far as the polymeric matrix/carriers are concerned, they were all amorphous, since HPC-SL showed an amorphous halo at $2\theta = 15\text{-}25°$, PVP displayed two broad halos in the region of $2\theta = 5\text{-}40°$, while SOL exhibited an amorphous halo in the region of 5 to $35°$ 2θ. Finally, P407 showed two (2) characteristic x-ray diffraction peaks at $19.2°$ and $23.3°$ over a broad amorphous halo, indicative of its semi-crystalline nature, while neat TPGS was also semi-crystalline with two characteristic pXRD peaks at $19.0°$ and $22.8°$. In respect to ASDs, Fig. 3b
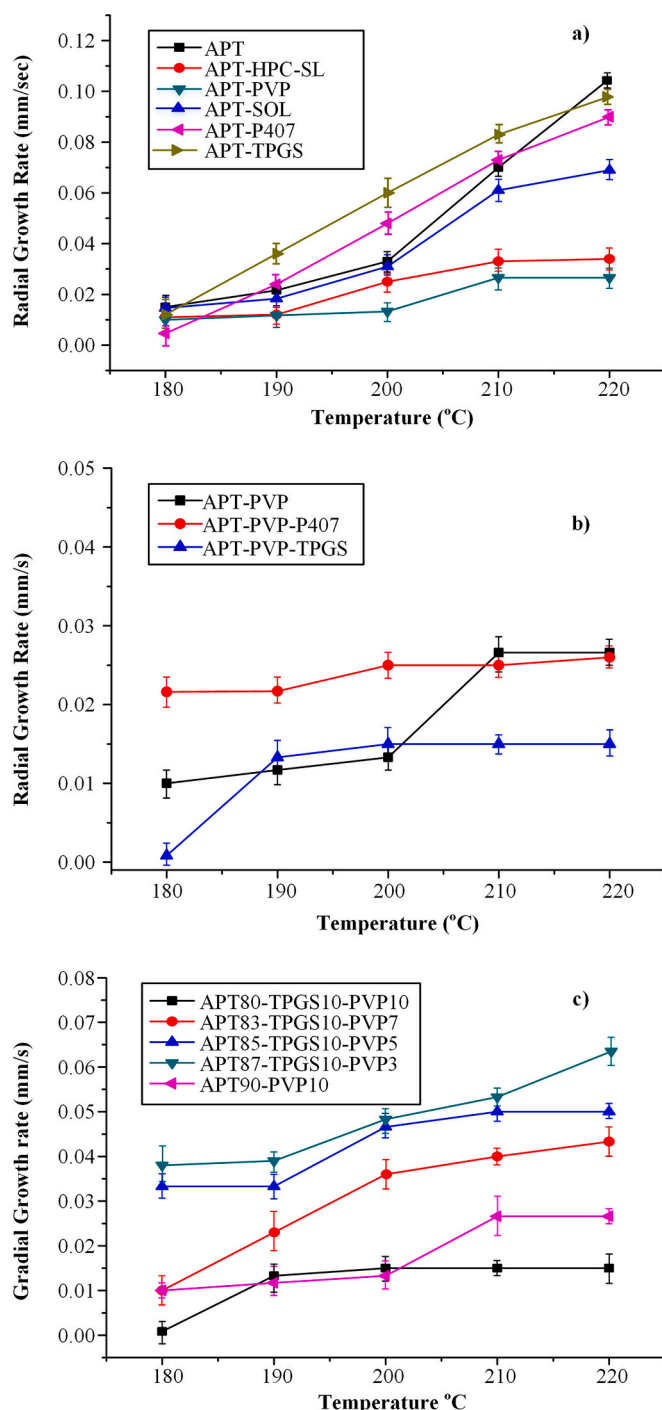

Fig. 4. Crystal growth rates of pure APT and APT's binary systems (a), APT-PVP system in the presence and absence of surfactant**s** (b), and APT-TPGS-PVP system in different PVP concentrations (c).

showed the pXRD diffractograms shortly after preparation (zero-time). Results showed that in all cases amorphous SDs were formed, since no API characteristic reflection peaks were recorded in the obtained zero-time patterns, confirming in this way the results derived from the 2nd DSC heating scan analysis discussed at Section 3.2.

3.5. Effect of surfactants on ternary ASDs

After ensuring that APT is amorphously dispersed within the prepared systems, the effect of surfactants on the performance and

characteristics of the ternary ASDs will be thoroughly evaluated. As stated in the introduction part, the presence of surfactants in such ternary systems may affect the stability of the API (i.e., its recrystallization tendency) in storage and during solubilization (i.e., dissolution). Therefore, in the following section the effect of both surfactants (i.e., P407 and TPGS) on the prepared ASDs will be evaluated in terms of API's recrystallization growth rate (a measurement related to the drug's stability during storage) and dissolution-driven nucleation induction time (a measurement related to API's stability during solubilization).

3.5.1. APT's crystal growth rate analysis

API's crystal growth rate measurements were utilized in order to evaluate the effect of surfactants on the physical state of APT during storage. In general, such measurements may be considered as fast pre-formulation screening studies that are able to identify the magnitude of factors (in this case the surfactants) on the recrystallization tendency of the API (Mosquera-Giraldo et al., 2014). Additionally, with these measurements, conclusions regarding the synergistic or antagonistic effect of ASD's matrix components (i.e., polymers and surfactants) on the API re-crystallization profile, may also be drawn.

Fig. 4a illustrates the crystal growth rate of the API in the absence of any additive, as well as in the presence of a single polymeric carrier or a surfactant (at a ratio of 90/10 w/w APT to carrier/surfactant). It is noteworthy that, according to the previously discussed DSC results, APT may be considered as a non-stable glass former (following Baird et al. classification system (Baird et al., 2010)) and hence, it is expected that
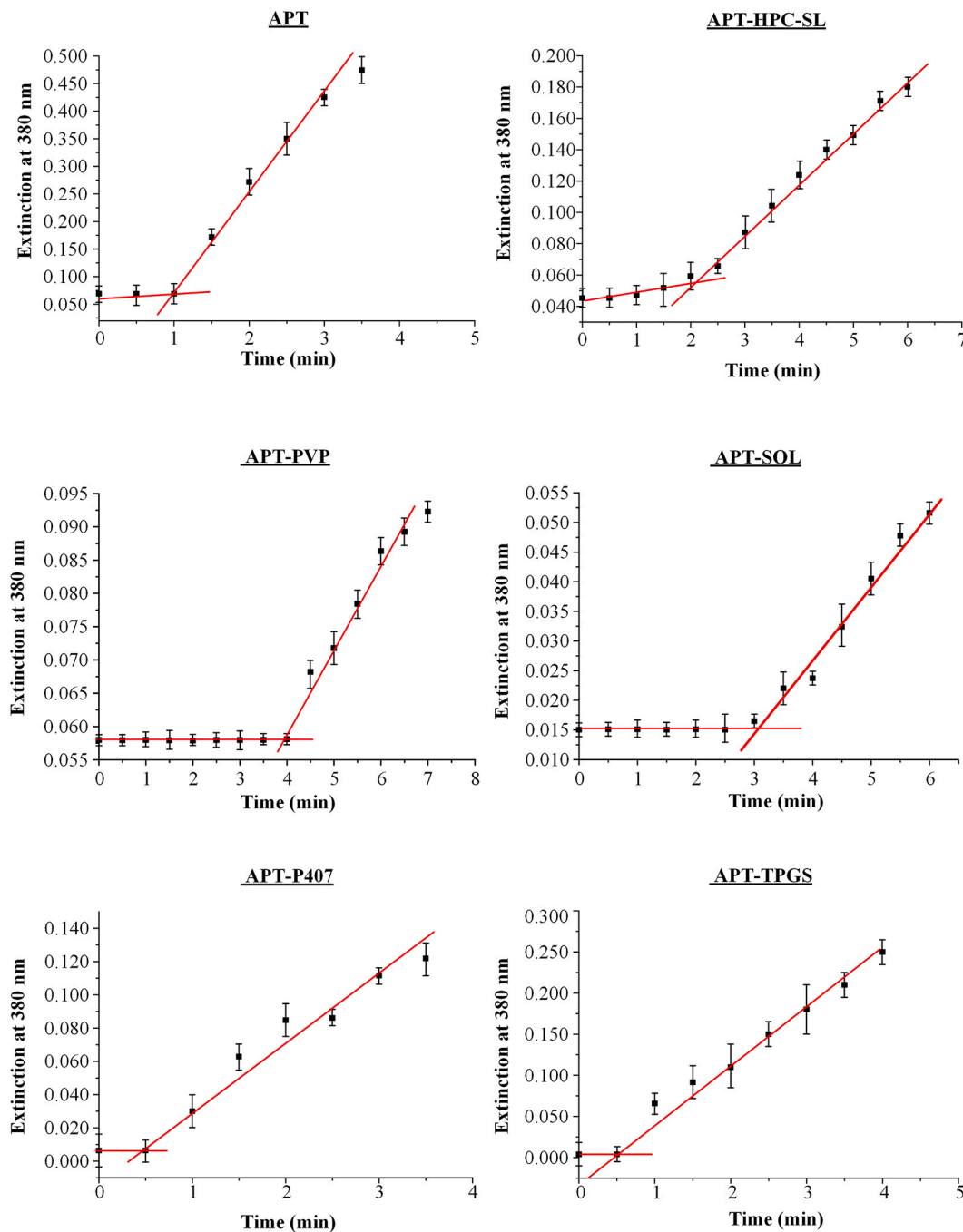

Fig. 5. Induction time measurements of APT in the absence and the presence of polymeric matrix-carriers (HPC-SL, PVP and SOL) and surfactants (P407 and TPGS) for S = 5.

the API is probably forming quite unstable amorphous glasses (Kapourani et al., 2020b). This assumption was confirmed from the obtained results, whereas the seeds of the crystalline API lead effortlessly to the nucleation and, subsequently, the crystal growth of the API in all experiments. Additionally, results in the same figure showed that increasing temperatures result in increasing drug crystal growth rates in all tested systems. The presence of each of the examined polymers reduced, without any exception, APT's crystal growth rate, while, contrariwise, in all tested temperatures (with the exception of 180 and 220 °C) the addition of surfactants resulted in higher crystal growth rates as compared to the pure API. Interestingly, the incorporation of PVP into the system brought about the most remarkable reduction of the APT's crystal growth rate (especially when the temperature increased), contrary to TPGS which had the greatest impact on increasing the rate of amorphous APT recrystallization.

In a further step, since PVP appeared to be the most suitable polymeric matrix-carrier, the growth rate of APT in the ternary ASDs using PVP and surfactants (at a ratio of 80/10/10 w/w of API/carrier/surfactant) was further evaluated. According to Fig. 4b, at temperatures over the range of 180–200 °C the incorporation of P407 into the binary APT-PVP system resulted in an increase of API's crystal growth rate; but at higher temperatures (i.e., 210-220 °C) the use of P407 did not have any remarkable impact on drug's recrystallization process (as compared to the respective binary system). On the contrary, in the presence of TPGS the crystal growth rate of APT at 180 °C, as well as at 210-220 °C, was noticeably decreased relatively to the binary APT-PVP system, while, regarding to the rest examined temperatures, the growth rate of the two systems (i.e., the binary APT-PVP and the ternary APT-PVP-TPGS) ranged at quite similar levels. Hence, based on the aforementioned results, it seems that even though TPGS increases APT's crystal growth rate when examined solely, its combination with PVP results in a significant reduction of API's recrystallization rate. It should be noted that similar results have been also reported for other drugs, such as in the case of celecoxib, where the presence of a surfactant increased API's crystal growth rate when tested alone, while a synergistic effect (i.e., further reduction in API's recrystallization rate) were recorded when a combination of the surfactant with a suitable polymeric matrix/carrier was evaluated (Mosquera-Giraldo et al., 2014).

Within this context, in an attempt to further evaluate the synergistic effect of PVP and TPGS, the crystal growth rates of APT in ternary systems containing 10 wt% TPGS combined with 3, 5 or 7 wt% PVP were also evaluated. Results in Fig. 4c showed that as the PVP concentration decreased from 10 to 3 wt%, the crystal growth rate of APT increased in all tested temperatures. As a result, the only system that presented improved growth rates, relatively to the binary APT-PVP ASD, was the one containing 10 wt% PVP. Regarding to the rest APT-PVP-TPGS systems presented in Fig. 4c, it seems that the crystal growth rate in the presence of the polymer and the surfactant is the average of the individual effects of the two components. Consequently, based on these findings, it is obvious that the selection of the ideal type and the optimum content of both polymer and surfactant in any such ternary ASD formulation, requires extreme attention and intensive pre-screening evaluation.

3.5.2. Evaluation of APT's nucleation induction time during dissolution

Surfactants are amphiphilic compounds containing different moieties. The polar and non-polar groups include a hydrophilic head and hydrophobic tail, respectively. In polar solvents, monomers, when they are presented above a specific concentration, they can self-assemble into clusters called micelles. Specifically, the hydrophobic part of the aggregate forms the core of the micelle, while the polar head groups are located at the micelle–water. The concentration at which the formation of micelles occurs is defined as the critical micelle concentration (CMC) (Dominguez et al., 1997; Kile and Chiou, 1989). A micelle is the simplest assembled entity, with well-defined molecular structures. However, one significant challenge that needs to be overcome during their utilization

in drug delivery formulations, is their low stability when environmental changes take place, since at a concentration below CMC, micelles can disassociate (Kim et al., 2010; Lu et al., 2018). Hence, the knowledge of the CMC of the surfactant used in the ternary ASDs is of crucial importance when evaluating the API's solubilization.

In the current study, since the presence of the API may alter the CMC values of surfactants, the true CMC of P407 and TPGS in the presence of APT was determined by plotting API's solubility against surfactant's concentration. In this case, the CMC is estimated by defining the value that corresponds to the concentration of the surfactant at which an abrupt change in drug's solubility is observed. Hence, according to the obtained results presented in Fig. S2 (supplementary material) the CMC value of TPGS and P407 in the presence of APT was 150 ppm and 40 ppm, respectively. It is noteworthy that, in both cases the obtained results are in good agreement with the values reported previously for the CMC of surfactants without the presence of additives (Grimaudo et al., 2018; Suksiriworapong et al., 2014), indicating that the CMC values were not significantly affected by the presence of the API.

Moving on with the evaluation of surfactant's impact on the API's stability during solubilization, it must be noted that, in general, the dissolution of any drug from ASDs is, typically, rapid, resulting in an initial surge of drug concentration in the dissolution medium, followed by a decline, due to the nucleation and crystallization events triggered by the rapid buildup of drug supersaturation (Sun and Lee, 2015). Consequently, API's recrystallization during the dissolution process is one of the most significant barriers that needs to be surpassed and, in order this to be achieved, the comprehension of the underlying mechanisms of crystallization is of great importance.

The crystallization tendency of the API within a supersaturated solution can be evaluated from its nucleation-induction time, according to the process described at Section 2.8. The induction time is defined as the elapsed time between the creation of the supersaturation and the appearance of detectable nuclei at a constant temperature. The turbidity measurement method used in this study provides an inexpensive and reliable technique for the measurement of induction time and has been commonly adopted in recent years (Kuldipkumar et al., 2007). The obtained results from all examined systems for $S = 5$ (i.e., initial supersaturation conditions were five times the equilibrium concentration of the crystalline APT) are presented at Fig. 5. The induction time, t_{ind}, was determined by plotting extinction versus time and drawing regression lines through the two distinct linear regions. The intersection point of regression lines for these two regions was taken as the t_{ind}. It should be noted that, API's concentration into the solution maintained its stability until the nucleation. From this point forward, the turbidity of the solution begins to increase, and a simultaneous rapid decrease of API's concentration takes place, as indicated by the UV absorption peaks. According to the obtained diagrams, the average induction time of APT in the absence of any additive was 1 min, while the additive that increased t_{ind} by the greatest extent was PVP (from 1 min to 4 min). It was clear that in the absence of any polymer, nucleation was rapid, and the drug concentration decreased rapidly whereby crystallization commenced. Additionally, both HPC-SL and SOL were able to increase the induction time, from 1 min to approximately 2 and 3 min, respectively. On the contrary, in the presence of P407 and TPGS the induction time was decreased to approximately 0.5 min. Consequently, it appears that the most effective crystal inhibitor of APT during supersaturation is PVP, while both surfactants lack such inhibiting efficiency. Additionally, when a lower initially degree of supersaturation was tested similar results were also recorded with PVP resulting in the slowest t_{ind} as compared to the rest components, and both TPGS and P407 leading to faster APT's nucleation induction times as compared to the neat API. These findings were in agreement with the results obtained from the crystal growth measurements of binary API mixtures, where the crystal growth rate of the API was significantly increased in the presence of surfactants, while PVP resulted in the most significant rate reduction.

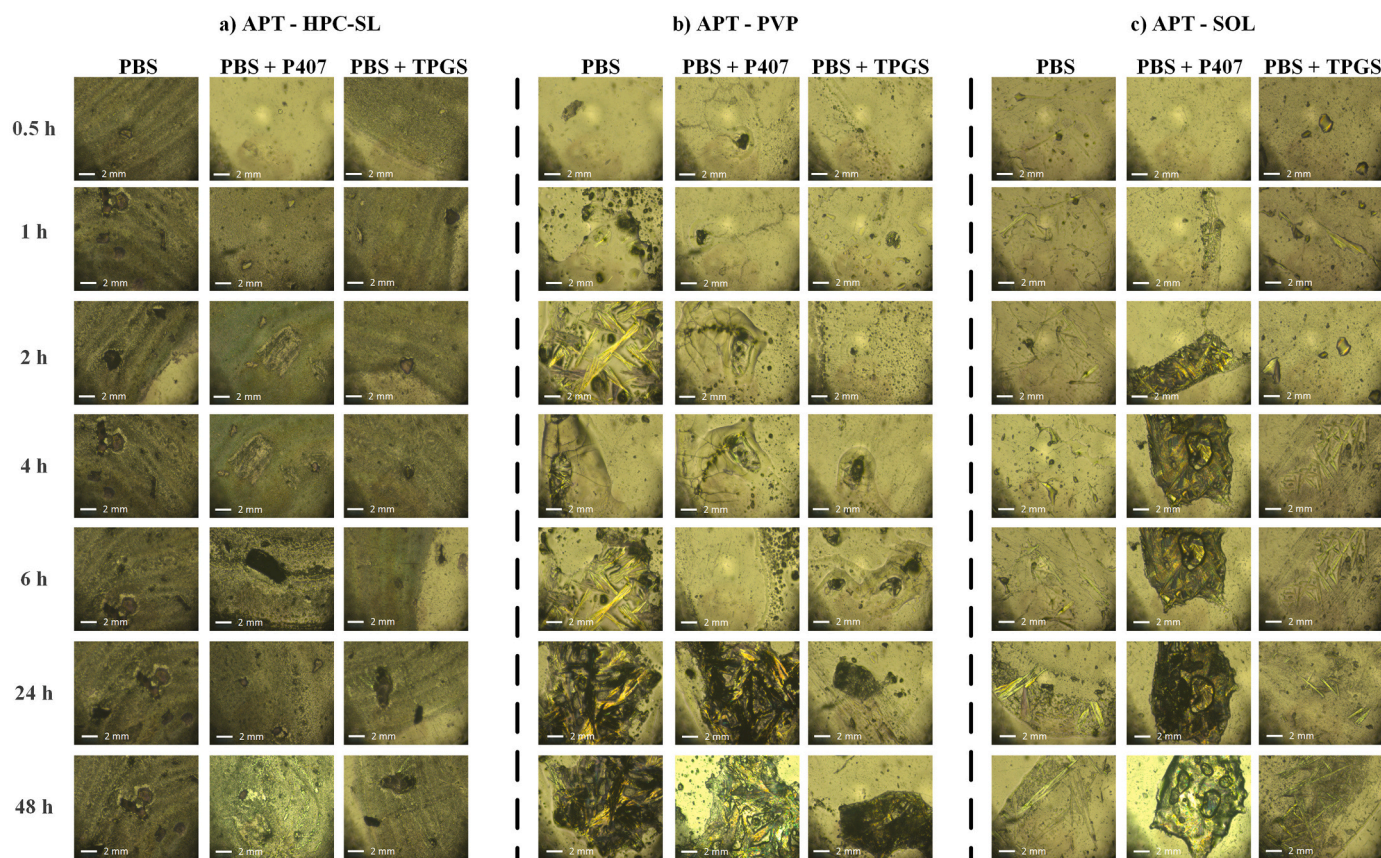In addition to nucleation induction time, the formation of API

a) APT - HPC-SL   **b) APT - PVP**   **c) APT - SOL**

Fig. 6. Suspension PLM photographs of: a) APT-HPC-SL ASD, b) APT-PVP ASD, and c) APT-SOL ASD (at a ratio of 30/70% w/w API to polymer) in different liquid media after 0.5, 1, 2, 4, 6, 24 and 48 h.

Table 1
Time at which APT recrystallization appeared when binary drug-polymer ASDs where immersed in pure PBS and PBS-surfactant solutions ('x' and '-' present the presence and absence of drug crystals, respectively).

Sample	Time duration in the respective dissolution medium						
	0.5 h	1 h	2 h	4 h	6 h	24 h	48 h
APT-HPC-SL							
PBS	–	–	–	x	x	x	x
PBS + P407	–	–	–	x	x	x	x
PBS + TPGS	–	–	–	x	x	x	x
APT-PVP							
PBS	–	x	x	x	x	x	x
PBS + P407	–	x	x	x	x	x	x
PBS + TPGS	–	–	–	–	–	x	x
APT-SOL							
PBS	–	–	–	x	x	x	x
PBS + P407	–	x	x	x	x	x	x
PBS + TPGS	–	–	–	x	x	x	x

crystals during the dissolution of APT ASDs was evaluated via PLM. Fig. 6 illustrates the recrystallization of APT from the binary polymeric ASDs when immersed in PBS or PBS-surfactant (P407 or TPGS) solutions, at several time points, while Table 1 summarizes in tubular form, the time at which the drug crystals appeared in the respective solution. According to the obtained images, in the case of pure PBS (i.e., without the addition of any surfactant) the highest and faster recrystallization took place with APT-PVP ASDs, while APT-HPC-SL and APT-SOL ASDs presented a noticeable recrystallization-resistance. When P407 was added, APT-PVP and APT-HPC-SL binary ASDs showed similar drug's recrystallization as in the case of PBS, while APT-SOL showed a

remarkable recrystallization enhancement, indicating that in the presence of the said surfactant, the initial inhibition of API's recrystallization, induced by the copolymer, was reversed. Finally, in the case of TPGS results showed no significant changes in API's recrystallization tendency when APT-HPC-SL and APT-SOL ASDs were tested (as compared to the pure PBS), while the addition of TPGS managed to significantly inhibit the recrystallization of the API in the case of APT-PVP binary dispersions. Hence, similarly to the previous results regarding APT's recrystallization during storage, it seems that the addition of TPGS in the binary APT-PVP ASDs significantly improves the resistance of API's recrystallization during dissolution, revealing, thus, once again, the synergy of TPGS and PVP as amorphous drug stabilizers.

Looking at the results obtained from the conducted dynamic studies (i.e., nucleation and crystallization rates) it seems that the type of surfactant used significantly affects ASDs' stability both during storage and solubilization (i.e., dissolution). In sum, although both surfactants tested (i.e., P407 and TPGS) resulted in a deterioration of APT's physical stability profile, the combination of TPGS with PVP showed a remarkable improvement in all aspects (resulting in significantly lower drug's crystal growth and nucleation induction rates). Also, focusing on the synergistic effect of PVP and TPGS, results revealed that the matrix/carrier content (i.e., PVP's weight ratio) significantly affects drug's recrystallization rate (a measurement related to the drug's stability during storage), with concentrations of PVP below 10% of the total formulation weight, resulting in a significant increase of APT's recrystallization tendency. Additionally, it is important to note that the onset of APT's nucleation, determined from the increase in intensity of light scattered from the drug solutions, was significantly faster as compared to the crystals' formation, depicted from the PLM study using PBS or PBS-surfactant solutions, indicating that there was a significant difference between the API's nuclei and the crystal growth rates in all the tested formulation
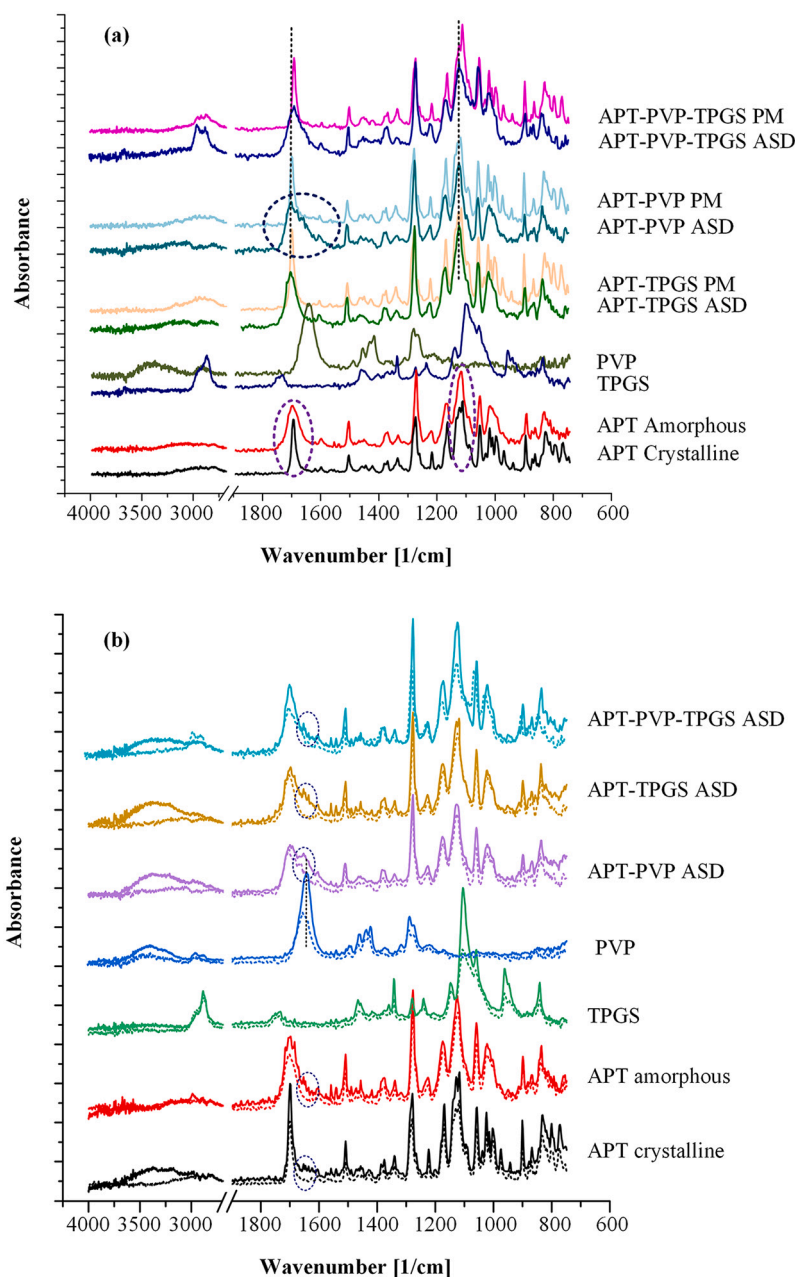
Fig. 7. ATR-FTIR spectra of: a) the initially used raw materials, the pure amorphous APT, the binary and ternary drug physical mixtures (PMs) and ASDs for APT-PVP-TPGS; and b) the respective anhydrous (dashed lines) and hydrated (solid lines) systems.

(the former being significantly faster). Finally, it should be pointed out that, since all above studies were comparative, it was not feasible to identify any critical values regarding the optimum ranges for the rate of drug's nucleation and recrystallization. On the contrary, what was revealed from the obtained results was the impact that the several formulation parameters studied (i.e., the type of matrix/carrier and surfactant, as well as their weight ratio) had on either enhancing or decreasing these rates.

3.6. Molecular interactions evaluation

3.6.1. ATR-FTIR studies

Since intermolecular interactions play a crucial role in the preparation and performance of any ASD system, their presence in the ternary APT- PVP-TPGS ASDs was evaluated via ATR-FTIR, in an attempt to explain the unexpected synergistic effect between the polymer and

surfactant. Fig. 7a presents the ATR-FTIR spectra of the initially used raw materials, the neat amorphous API (prepared by melt-quench cooling), the binary API physical mixtures (PMs, prepared by mixing via mortar and pestle) and the respective ASDs.

In regard to the neat crystalline APT, the recorded ATR-FTIR spectrum showed all characteristic FTIR peaks of the form I and II crystals corresponding to the -C=O stretching at 1701 cm^{-1}, -C-F stretching at 1126 and 1115 cm^{-1} and -C=C- stretching at 1600 to 1500 cm^{-1}. As for the differences between the crystalline and the amorphous API, the latter showed several noticeable shifts in the region of 1750 to 1650 cm^{-1} and 1126 to 1115 cm^{-1} (both depicted with a purple dashed cycle in the respective figure), corresponding to the -C=O and -C-F vibrations, respectively. Looking more closely in previous published results regarding the crystalline lattices of APT's polymorphs I and II, it was realized that in both arrangements two strong independent N—H⋯O hydrogen bonds (HBs) are being formed (Braun et al., 2008).
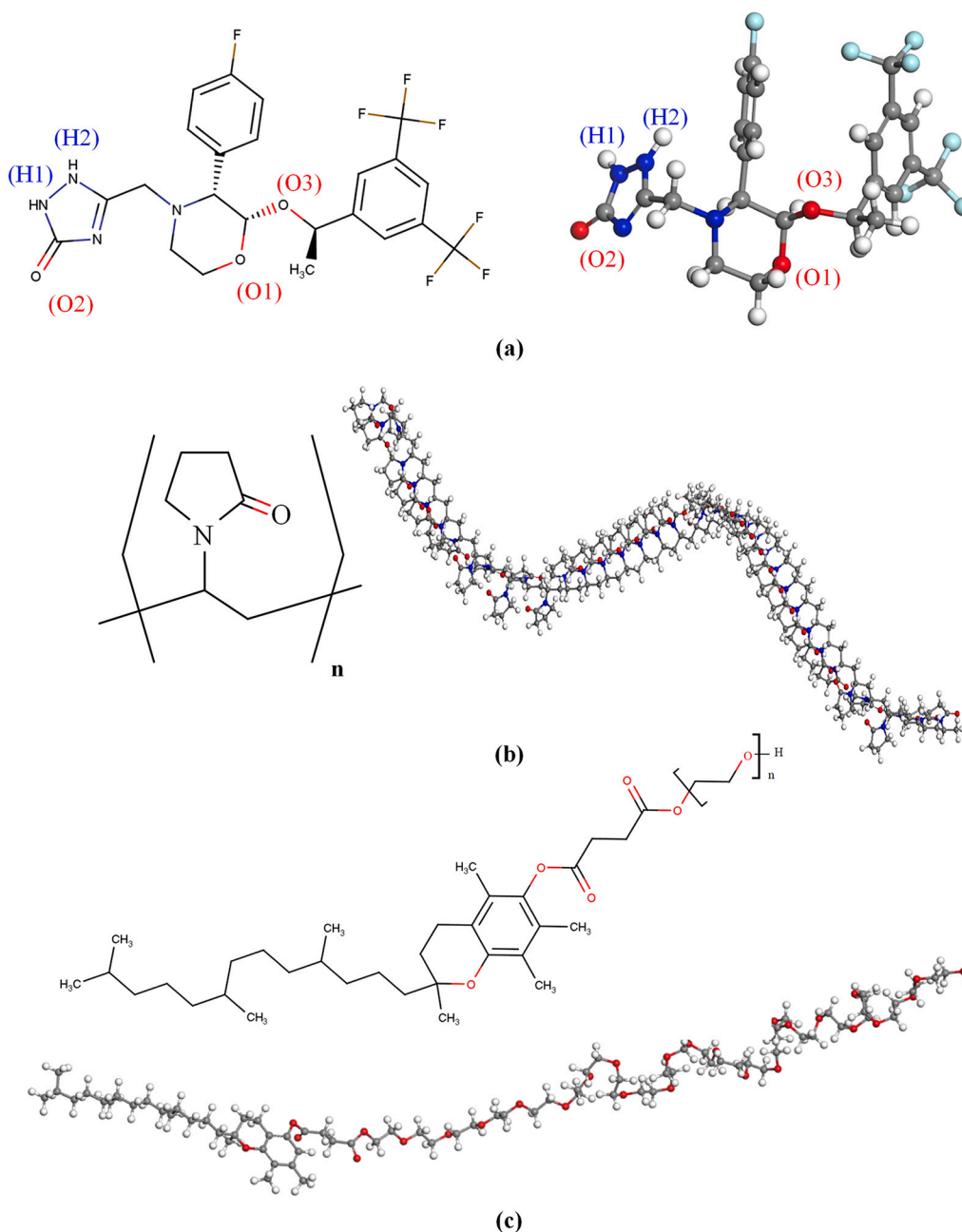
Fig. 8. Chemical structures of APT (a), PVP (b) and TPGS (c) used during the MD simulations (hydrogen atoms are depicted with white, carbon atoms with grey, oxygen atoms with red, nitrogen atoms with blue and fluorine atoms with cyan). (For interpretation of the references to colour in this figure legend, the reader is referred to the web version of this article.)

Additionally, a number of weak, non-standard interactions of the C—H···F type were also recorded in both forms, while additional weak interactions of the C—H···F type are also found in APT form I crystals (Braun et al., 2008). Hence, based on these results, the differences observed in the ATR-FTIR spectrum of the amorphous API, are probably due to different N—H···O and C—H···F molecular interactions occurring between the API molecules within their different physical states.

Regarding the rest raw materials, the obtained spectra showed all ATR-FTIR characteristic vibration peaks. Specifically, in the case of neat PVP characteristic ATR-FTIR peaks were recorded at 3425 cm^{-1} (corresponding to absorbed water), 2968 cm^{-1} (corresponding to ν(C—H)), 1647 cm^{-1} (corresponding to ν(C=O), 1461 and 1420 cm^{-1} (corresponding to (δCH$_2$)) and 1288 cm^{-1} (corresponding to ν(C—N)), while TPGS showed a characteristic FTIR peak at 2885 cm^{-1} (due to aromatic

C—H stretching vibration) and a second vibration peak at 1730 cm^{-1} (due to ester C=O stretching).

Looking at the recorded binary and ternary ATR-FTIR spectra of the prepared PMs, it is seen that in all cases the collected spectra were the sum of the individual crystalline API and the respective additive's spectra (i.e., polymer or surfactant). This finding suggests that among the PM's individual components no chemical interactions were formed. Additionally, during the preparation of the PMs the API remained crystalline since no API amorphous ATR-FTIR peaks were recorded. On the contrary, in the case of APT's binary ASDs (i.e., APT-PVP and APT-TPGS ASDs) the collected ATR-FTIR spectra were clearly the sum of the respective matrix/carrier and the amorphous API (all characteristic amorphous APT vibrations peaks at ~1700 cm^{-1} and ~ 1120 cm^{-1} were recorded). However, it is important to note that in the case of APT-PVP
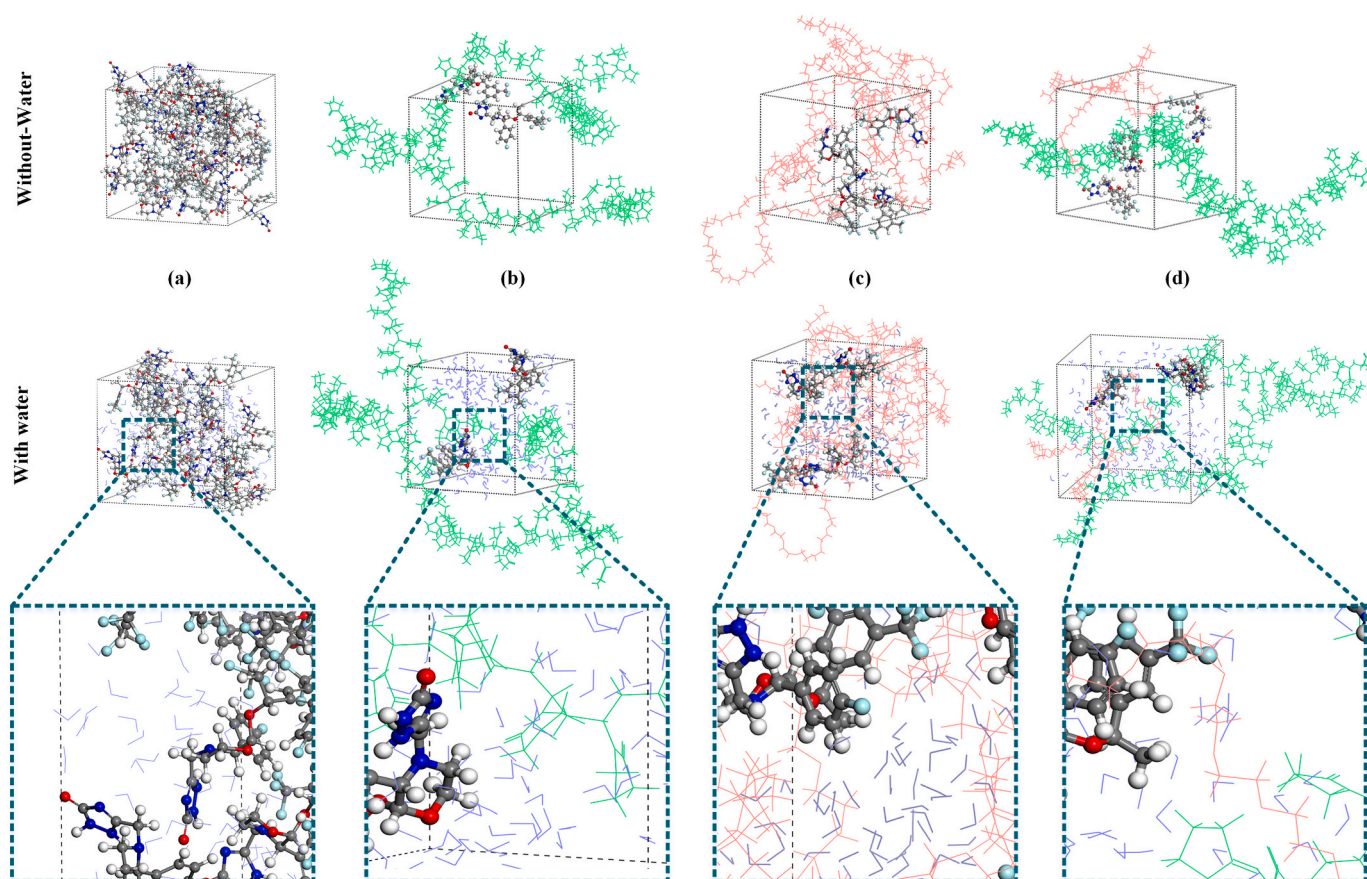
Fig. 9. MD simulation amorphous assemblies for APT (a) APT-PVP (b), APT-TPGS (c) and APT-PVP-TPGS (d) with or without the presence of water molecules. PVP and TPGS polymeric chains are depicted with green and red colors, respectively, while water molecules are depicted with purple. APT is shown in ball-stick style with hydrogen atoms depicted with white, carbon atoms with grey, oxygen atoms with red, nitrogen atoms with blue and fluorine atoms with cyan colors, respectively. A magnification of the amorphous assemblies is also given. (For interpretation of the references to colour in this figure legend, the reader is referred to the web version of this article.)

the ATR-FTIR peak corresponding to the -C=O (depicted in the dark blue dashed cycle) was clearly more widened compared to the neat amorphous API, indicating that probably significant intermolecular interactions were formed between the amorphous API and the polymeric matrix/carrier. These interactions, that were not observed in the case of APT-TPGS ASDs, are probably responsible for the diminution of API's re-crystallization in the presence of PVP.

Finally, in the case of APT ASDs containing both PVP and TPGS, the recorded ATR-FTIR spectrum was similar to the APT-PVP, indicating that similar intermolecular interactions were also formed in the ternary ASDs. However, a closer look at the peaks corresponding to the -C=O and -CF$_3$ vibrations of the amorphous API, showed a slight shift to lower wavenumbers as compared to the binary APT-PVP ASDs (depicted with a black vertical dashed line in the respective figure), indicating that the molecular interaction formed between the amorphous API and PVP were enhanced in the presence of TPGS. Hence, these stronger molecular interactions identified in the ternary ASDs, may, in some extent, explain the previously determined synergistic effect of PVP and TPGS in terms of API's crystal growth rate and nucleation induction time.

3.6.1.1. Molecular interactions evaluated after hydration. In addition, the evolving molecular interactions between system's components were also evaluated via ATR-FTIR after their hydration in PBS. In this way an insight into the interactions responsible for API's amorphous stabilization within the hydrated ASD systems will be gained. Fig. 7b depicts the overlay spectra of the anhydrous and the hydrated raw materials as well as those of the corresponding ASDs. Clearly, with the exemption of

TPGS, a broad FTIR peak corresponding to the presence of water was recorded at ~3700–3000 cm^{-1} in all cases, while the bending of water's O—H was also recorded at ~1640 cm^{-1} in all hydrated ASDs and both hydrated API samples (i.e., the amorphous and the crystalline APT). Additionally, as it can be seen in the same figure, during the hydration process the carbonyl band of PVP was shifted to lower wavenumbers, indicating that in the presence of water strong H-bonds are being formed between these two components. On the contrary, the spectra of the rest raw materials (i.e., the amorphous and crystalline APT and the TPGS) did not show any significant changes during hydration, indicating restricted interactions between these components and water. In the case of ASDs, and especially during the hydration process of the ternary APT-PVP-TPGS system, a significant reduction in water's O—H peak intensity at ~1640 cm^{-1} was recorded, as compared to the respecting APT-PVP binary ASD, indicating that in the presence of TPGS the hydration sites of the pure polymer are restricted (probably due to steric hindrance phenomena), limiting thus the effective molecular interactions between water and PVP (and subsequently, the whole solubilization process). Hence, this finding could explain (in some extent) the reduced APT's nucleation and crystal growth rates observed in the case of APT-PVP-TPGS ternary ASDs in the presence of water.

3.6.2. MD simulations

In addition to ATR-FTIR, the type of intermolecular interactions evolving between the API and the matrix components during the preparation of the ternary APT-PVP-TPGS ASDs and in the presence of water was also evaluated via MD simulations. Fig. 8 shows the initial
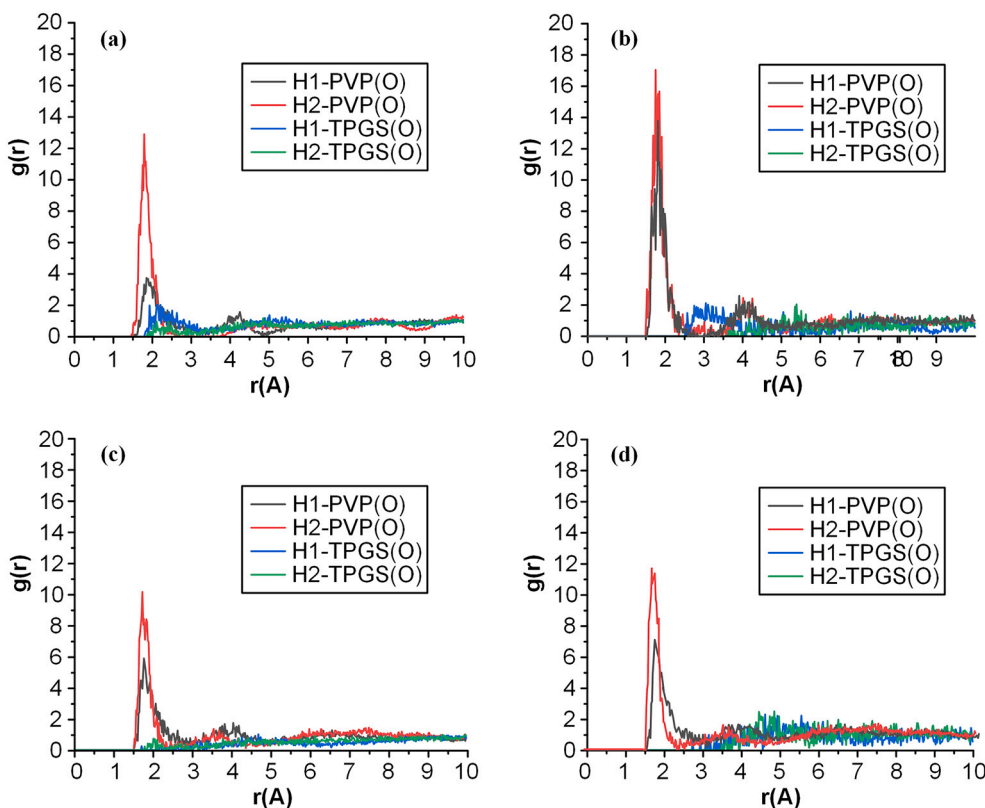
Fig. 10. Radial distribution function, g(r), between APT's -NH protons (H1 and H2) and PVP's or TPGS's HB acceptor oxygens (O) in anhydrous binary (a) or ternary (b) ASDs, as well as in hydrated binary (c) and ternary (d) systems (only intermolecular interactions are being depict in all cases).

molecular structures of all components, while Fig. 9 shows the constructed amorphous assemblies for the pure APT, the binary (i.e., APT-PVP and APT-TPGS) and the ternary (APT-PVP-TPGS) systems in the presence and absence of water. It should be noted that the initial molecular structure of APT was obtained from the Cambridge Structural Database (CSD Deposition Number: 117932) based on the published work of Hale et al. (Hale et al., 1998), while PVP's molecular chains (consisting of 40 N-vinylpyrrolidone monomers) were constructed based on a previous study of ours (Kapourani et al., 2020a), and TPGS's chains (consisting of 22 ethylene glycol monomers) were prepared based on the reported structure of tocophersolan (Pubchem, CID: 71406).

In the case of MD simulations (either in the presence or in the absence of water), the evaluation of intermolecular interactions was made by calculating the radial distribution function, g(r). In general, g(r) describes the correlation between atoms in a given system, and is calculated by the following equation:

$$g(r) = \frac{\langle V \Sigma_{i \neq j} \delta(r - |r_{Ai} - r_{Bi}|) \rangle}{(N_A N_B - N_{AB}) 4 \pi r^2 dr} \tag{1}$$

where A and B are specific atoms, V is the system volume, N_A and N_B are particle number of atoms A and B, respectively, N_{AB} are the number of particles belonging to atom A and atom B simultaneously, and r_{Ai} and r_{Bj} is the position of particle i of atom A particle j of atom B, respectively. Estimated g(r) donor-acceptor distances below 2.5 Å indicate the formation of strong interactions, distances between 2.5 and 3.2 Å indicate moderate, mostly electrostatic, interactions, while distances between 3.2 and 4.0 Å indicate weak, also electrostatic, interactions.

3.6.2.1. MD simulation during ASD's preparation (absence of water). Fig. 10a and b show the g(r) for APT's -NH protons (H1 and H2) and polymer's or surfactant's (i.e., PVP or TPGS) oxygens in the binary and ternary ASDs (only intermolecular interactions are being depict) in the

Table 2
Summary of g(r) peak positions calculated based on the MD simulation results either in the presence or the absence of water.

Interaction type	g(r) peak position (Å)			
	Without water		With water	
	Binary	Ternary	Binary	Ternary
APT(H1)-PVP(O)	1.81	2.05	1.92	2.12
APT(H2)-PVP(O)	1.75	1.83	1.87	1.94

absence of water, while Table 2 summarizes the most significant g(r) peak positions. In the case of binary ASDs, results in Fig. 10a showed two strong g(r) peaks for H1…PVP(O) and H2…PVP(O), respectively (at an r distance of 1.81 Å and 2.05 Å), indicating the formation of strong HBs between APT's -NH protons and PVP's -C=O during API's amorphization. Similarly, in the case of ternary ASDs the same HBs were also recorded, however, at a lower r distance (namely 1.75 Å and 1.83 Å), indicating that stronger intramolecular HBs were being formed between the API and the polymer in this case. Hence, based on the obtained results, it can be said that the MD simulations were in perfect agreement with the ATR-FTIR experimental findings, suggesting that stronger molecular interactions are being formed in the case of ternary APT-PVP-TPGS ASDs. In addition, MD simulations were able to unravel the type of these interactions, by identifying the formation of strong HBs between the API and the polymer. Finally, in an attempt to interpret these stronger interactions, it can be assumed that the melting of TPGS during the preparation of ASDs is probably setting the necessary liquid substrate for the API's molecules to come in closer contact and react with the oxygens of PVP (i.e., TPGS is acting as a better plasticizer to both PVP and APT). However, other factors including the wetting properties of the components, the HLB value of the surfactant etc., are probably contributing highly in the observed PVP-TPGS synergy.

3.6.2.2. MD simulations in the presence of water. In addition to the ASD's preparation, the evaluation of molecular interactions during system's solubilization (i.e., in the presence of water), is equally important in order to gain an insight into the mechanisms of water-induced API's nucleation and recrystallization processes. Fig. 10c and d show the calculated g(r) profiles for APT's -NH protons (H1 and H2) and polymer's or surfactant's (i.e., PVP or TPGS) oxygens, used in order to evaluate the changes in the molecular interactions evolving between the system's components in the presence of water. Additionally, all calculated g(r) peak positions estimated by the conducted MD simulations are summarized in Table 2. Based on the obtained results it is obvious that the strong H-bonds formed between the NH proton hydrogens of APT (i.e., H1 and H2) and PVP's C═O oxygens, are maintained in the presence of water, although lower values of g(r) are recorded as compared to the anhydrous systems, indicating that the formation of such strong intermolecular interactions is less favorable in the former case. Additionally, it is important to note that for the ternary ASD the obtained g(r) peaks corresponding to the formation of strong H-bonds between the API and PVP, are placed in a shorter r(A) distances and higher g(r) values as compared to the respective binary systems, indicating that in the presence of TPGS the APT-PVP intermolecular interactions are enhanced (due to PVP-TPGS synergistic effect). This finding may provide an explanation regarding the reduced APT's nucleation and crystal growth rates in the case of APT-PVP-TPGS ternary ASDs.

4. Conclusion

Despite the obvious upsurge of research into ternary ASDs, especially in the past recent years, there are several aspects of surfactant based ternary ASDs that need to be further examined (such as drug's physical stability and recrystallization tendency during supersaturation). Taking this into consideration, the aim of the present study was to gain a further insight into the field and evaluate the impact of various surfactants (P407 and TPGS) and matrix-carriers (HPC-SL, PVP and SOL) on the crystal growth rate and the mechanisms of crystallization tendency of APIs (APT). According to the obtained results all tested components were completely miscible, while DSC thermograms proved the plasticizing effect of both surfactants on APT. As far as the crystal growth rate studies are concerned, PVP had the greatest effect on decreasing the growth rate of amorphous APT, contrary to P407 and TPGS where the API's recrystallization rate was increased. Nonetheless, TPGS presented a significant synergistic effect when combined with PVP (leading to a further reduction of API's crystal growth rate), although this effect depended on polymer's concentration. Additionally, PVP proved as the most effective crystal inhibitor, when the induction time of APT in presence and in absence of polymers was evaluated, while a similar significant synergistic effect was observed when ternary APT-PVP-TPGS ASDs were examined. Finally, the formation of strong intermolecular interactions was identified (via ATR-FTIR) in the case of ternary ASDs containing APT, P*VP* and TPGS (providing thus, an explanation for the PVP-TPGS synergistic effect) while the utilization of MD simulation was able to unravel the type and extent of these interactions. In conclusion, based on the findings of the present study the selection of a proper surfactant for the preparation of ternary polymeric ASDs, requires remarkable attention and in-depth evaluation, as it is vital to examine the impact of each component, alone and in combination, through the execution of extensive pre-formulation studies, that will, eventually, save both time and effort during the development of such amorphous drug dispersions.

Declaration of Competing Interest

The authors report no declarations of interest.

Appendix A. Supplementary data

Supplementary data to this article can be found online at https://doi.org/10.1016/j.ijpx.2021.100086.

References

Baird, J.A., Van Eerdenbrugh, B., Taylor, L.S., 2010. A classification system to assess the crystallization tendency of organic molecules from undercooled melts. J. Pharm. Sci. 99, 3787–3806.

Barmpalexis, P., Grypioti, A., Eleftheriadis, G.K., Fatouros, D.G., 2018a. Development of a new aprepitant liquisolid formulation with the aid of artificial neural networks and genetic programming. AAPS PharmSciTech 19, 741–752.

Barmpalexis, P., Karagianni, A., Kachrimanis, K., 2018b. Molecular simulations for amorphous drug formulation: polymeric matrix properties relevant to hot-melt extrusion. Eur. J. Pharm. Sci. 119, 259–267.

Barmpalexis, P., Karagianni, A., Katopodis, K., Vardaka, E., Kachrimanis, K., 2019. Molecular modelling and simulation of fusion-based amorphous drug dispersions in polymer/plasticizer blends. Eur. J. Pharm. Sci. 130, 260–268.

Ben Osman, Y., Liavitskaya, T., Vyazovkin, S., 2018. Polyvinylpyrrolidone affects thermal stability of drugs in solid dispersions. Int. J. Pharm. 551, 111–120.

Braun, D.E., Gelbrich, T., Kahlenberg, V., Laus, G., Wieser, J., Griesser, U.J., 2008. Packing polymorphism of a conformationally flexible molecule (aprepitant). New J. Chem. 32, 1677–1685.

Chaudhari, S.P., Dugar, R.P., 2017. Application of surfactants in solid dispersion technology for improving solubility of poorly water soluble drugs. J. Drug Deliv. Sci. Technol. 41, 68–77.

Chen, J., Ormes, J.D., Higgins, J.D., Taylor, L.S., 2015. Impact of surfactants on the crystallization of aqueous suspensions of celecoxib amorphous solid dispersion spray dried particles. Mol. Pharm. 12, 533–541.

Chen, Y., Wang, S., Wang, S., Liu, C., Su, C., Hageman, M., Hussain, M., Haskell, R., Stefanski, K., Qian, F., 2016. Sodium lauryl sulfate competitively interacts with HPMC-AS and consequently reduces oral bioavailability of posaconazole/HPMC-AS amorphous solid dispersion. Mol. Pharm. 13, 2787–2795.

Davis, M.T., Potter, C.B., Walker, G.M., 2018. Downstream processing of a ternary amorphous solid dispersion: the impacts of spray drying and hot melt extrusion on powder flow, compression and dissolution. Int. J. Pharm. 544, 242–253.

Deshpande, T.M., Shi, H., Pietryka, J., Hoag, S.W., Medek, A., 2018. Investigation of polymer/surfactant interactions and their impact on itraconazole solubility and precipitation kinetics for developing spray-dried amorphous solid dispersions. Mol. Pharm. 15, 962–974.

Dominguez, A., Fernandez, A., Gonzalez, N., Iglesias, E., Montenegro, L., 1997. Determination of critical micelle concentration of some surfactants by three techniques. J. Chem. Educ. 74, 1227.

Feng, D., Peng, T., Huang, Z., Singh, V., Shi, Y., Wen, T., Lu, M., Quan, G., Pan, X., Wu, C., 2018. Polymer⁻surfactant system based amorphous solid dispersion: precipitation inhibition and bioavailability enhancement of itraconazole. Pharmaceutics 10, 53.

Fule, R., Amin, P., 2014. Development and evaluation of lafutidine solid dispersion via hot melt extrusion: investigating drug-polymer miscibility with advanced characterisation. Asian J. Pharm. Sci. 9, 92–106.

Fule, R., Meer, T., Amin, P., Dhamecha, D., Ghadlinge, S., 2014. Preparation and characterisation of lornoxicam solid dispersion systems using hot melt extrusion technique. J. Pharm. Investig. 44, 41–59.

Ghebremeskel, A.N., Vemavarapu, C., Lodaya, M., 2007. Use of surfactants as plasticizers in preparing solid dispersions of poorly soluble API: selection of polymer–surfactant combinations using solubility parameters and testing the processability. Int. J. Pharm. 328, 119–129.

Gibaldi, M., Feldman, S., Wynn, R., Weiner, N.D., 1968. Dissolution rates in surfactant solutions under stirred and static conditions. J. Pharm. Sci. 57, 787–791.

Goddeeris, C., Willems, T., Houthoofd, K., Martens, J.A., Van den Mooter, G., 2008. Dissolution enhancement of the anti-HIV drug UC 781 by formulation in a ternary solid dispersion with TPGS 1000 and Eudragit E100. Eur. J. Pharm. Biopharm. 70, 861–868.

Grimaudo, M.A., Pescina, S., Padula, C., Santi, P., Concheiro, A., Alvarez-Lorenzo, C., Nicoli, S., 2018. Poloxamer 407/TPGS mixed micelles as promising carriers for cyclosporine ocular delivery. Mol. Pharm. 15, 571–584.

Gunsteren, W.F.V., Mark, A.E., 1998. Validation of molecular dynamics simulation. J. Chem. Phys. 108, 6109–6116.

Hale, J.J., Mills, S.G., MacCoss, M., Finke, P.E., Cascieri, M.A., Sadowski, S., Ber, E., Chicchi, G.G., Kurtz, M., Metzger, J., Eiermann, G., Tsou, N.N., Tattersall, F.D., Rupniak, N.M.J., Williams, A.R., Rycroft, W., Hargreaves, R., MacIntyre, D.E., 1998. Structural optimization affording 2-(R)-(1-(R)-3,5-Bis(trifluoromethyl) phenylethoxy)-3-(S)-(4-fluoro)phenyl-4- (3-oxo-1,2,4-triazol-5-yl) methylmorpholine, a potent, orally active, long-acting morpholine acetal human NK-1 receptor antagonist. J. Med. Chem. 41, 4607–4614.

Ilevbare, G.A., Taylor, L.S., 2013. Liquid–liquid phase separation in highly supersaturated aqueous solutions of poorly water-soluble drugs: implications for solubility enhancing formulations. Cryst. Growth Des. 13, 1497–1509.

Janssens, S., Van den Mooter, G., 2009. Review: physical chemistry of solid dispersions. J. Pharm. Pharmacol. 61, 1571–1586.

Kapourani, A., Vardaka, E., Katopodis, K., Kachrimanis, K., Barmpalexis, P., 2019. Rivaroxaban polymeric amorphous solid dispersions: moisture-induced thermodynamic phase behavior and intermolecular interactions. Eur. J. Pharm. Biopharm. 145, 98–112.

Kapourani, A., Chatzitheodoridou, M., Kontogiannopoulos, K.N., Barmpalexis, P., 2020a. Experimental, thermodynamic, and molecular modeling evaluation of amorphous simvastatin-poly(vinylpyrrolidone) Solid dispersions. Mol. Pharm. 17, 2703–2720.

Kapourani, A., Vardaka, E., Katopodis, K., Kachrimanis, K., Barmpalexis, P., 2020b. Crystallization tendency of APIs possessing different thermal and glass related properties in amorphous solid dispersions. Int. J. Pharm. 579, 119149.

Karataş, A., Yüksel, N., Baykara, T., 2005. Improved solubility and dissolution rate of piroxicam using gelucire 44/14 and labrasol. Il Farmaco 60, 777–782.

Kile, D.E., Chiou, C.T., 1989. Water solubility enhancements of DDT and trichlorobenzene by some surfactants below and above the critical micelle concentration. ES T Cont. 23, 832–838.

Kim, S., Shi, Y., Kim, J.Y., Park, K., Cheng, J.-X., 2010. Overcoming the barriers in micellar drug delivery: loading efficiency, in vivo stability, and micelle–cell interaction. Exp. Opin. Drug Deliv. 7, 49–62.

Kojima, T., Higashi, K., Suzuki, T., Tomono, K., Moribe, K., Yamamoto, K., 2012. Stabilization of a supersaturated solution of mefenamic acid from a solid dispersion with EUDRAGIT® EPO. Pharm. Res. 29, 2777–2791.

Kuldipkumar, A., Kwon, G.S., Zhang, G.G.Z., 2007. Determining the growth mechanism of tolazamide by induction time measurement. Cryst. Growth Des. 7, 234–242.

Kyaw Oo, M., Mandal, U.K., Chatterjee, B., 2017a. Polymeric behavior evaluation of PVP K30-poloxamer binary carrier for solid dispersed nisoldipine by experimental design. Pharm. Dev. Technol. 22, 2–12.

Kyaw Oo, M., Mandal, U.K., Chatterjee, B., 2017b. Polymeric behavior evaluation of PVP K30-poloxamer binary carrier for solid dispersed nisoldipine by experimental design. Pharm. Dev. Technol. 22, 2–12.

Lang, B., Liu, S., McGinity, J.W., Williams, R.O., 2016. Effect of hydrophilic additives on the dissolution and pharmacokinetic properties of itraconazole-enteric polymer hot-melt extruded amorphous solid dispersions. Drug Dev. Ind. Pharm. 42, 429–445.

Liu, C., Chen, Z., Chen, Y., Lu, J., Li, Y., Wang, S., Wu, G., Qian, F., 2016. Improving oral bioavailability of sorafenib by optimizing the "spring" and "parachute" based on molecular interaction mechanisms. Mol. Pharm. 13, 599–608.

Lu, Y., Yue, Z., Xie, J., Wang, W., Zhu, H., Zhang, E., Cao, Z., 2018. Micelles with ultralow critical micelle concentration as carriers for drug delivery. Nat. Biomed. Eng. 2, 318–325.

Ma, X., Williams, R.O., 2019. Characterization of amorphous solid dispersions: an update. J. Drug Deliv. Sci. Technol. 50, 113–124.

Meng, F., Meckel, J., Zhang, F., 2017. Investigation of itraconazole ternary amorphous solid dispersions based on povidone and Carbopol. Eur. J. Pharm. Sci. 106, 413–421.

Meng, F., Ferreira, R., Zhang, F., 2019. Effect of surfactant level on properties of celecoxib amorphous solid dispersions. J. Drug Deliv. Sci. Technol. 49, 301–307.

Moes, J.J., Koolen, S.L.W., Huitema, A.D.R., Schellens, J.H.M., Beijnen, J.H., Nuijen, B., 2011. Pharmaceutical development and preliminary clinical testing of an oral solid dispersion formulation of docetaxel (ModraDoc001). Int. J. Pharm. 420, 244–250.

Mosquera-Giraldo, L.I., Trasi, N.S., Taylor, L.S., 2014. Impact of surfactants on the crystal growth of amorphous celecoxib. Int. J. Pharm. 461, 251–257.

Nanaki, S., Eleftheriou, R.M., Barmpalexis, P., Kostoglou, M., Karavas, E., Bikiaris, D., 2019. Evaluation of dissolution enhancement of aprepitant drug in ternary pharmaceutical solid dispersions with Soluplus® and Poloxamer 188 prepared by melt mixing. Sci 1, 48.

Newman, A., Engers, D., Bates, S., Ivanisevic, I., Kelly, R.C., Zografi, G., 2008. Characterization of amorphous API:Polymer mixtures using X-ray powder diffraction. J. Pharm. Sci. 97, 4840–4856.

Pedretti, A., Villa, L., Vistoli, G., 2004. VEGA – an open platform to develop chemo-bio-informatics applications, using plug-in architecture and script programming. J. Comput. Aided Mol. Des. 18, 167–173.

Pham, T.N., Watson, S.A., Edwards, A.J., Chavda, M., Clawson, J.S., Strohmeier, M., Vogt, F.G., 2010. Analysis of amorphous solid dispersions using 2D solid-state NMR and 1H T1 relaxation measurements. Mol. Pharm. 7, 1667–1691.

Prasad, D., Chauhan, H., Atef, E., 2014. Amorphous stabilization and dissolution enhancement of amorphous ternary solid dispersions: combination of polymers showing drug–polymer interaction for synergistic effects. J. Pharm. Sci. 103, 3511–3523.

Qian, F., Huang, J., Hussain, M.A., 2010. Drug–polymer solubility and miscibility: stability consideration and practical challenges in amorphous solid dispersion development. J. Pharm. Sci. 99, 2941–2947.

Singh, P., Desai, S.J., Flanagan, D.R., Simonelli, A.P., Higuchi, W.I., 1968. Mechanistic study of the influence of micelle solubilization and hydrodynamic factors on the dissolution rate of solid drugs. J. Pharm. Sci. 57, 959–965.

Siriwannakij, N., Heimbach, T., Serajuddin, A.T.M., 2021. Aqueous dissolution and dispersion behavior of polyvinylpyrrolidone vinyl acetate-based amorphous solid dispersion of ritonavir prepared by hot-melt extrusion with and without added surfactants. J. Pharm. Sci. 110 (4), 1480–1494. https://doi.org/10.1016/j.xphs.2020.08.007.

Solanki, N.G., Lam, K., Tahsin, M., Gumaste, S.G., Shah, A.V., Serajuddin, A.T.M., 2019. Effects of surfactants on itraconazole-HPMCAS solid dispersion prepared by hot-melt extrusion I: miscibility and drug release. J. Pharm. Sci. 108, 1453–1465.

Suksiriworapong, J., Rungvimolsin, T., A-gomol, A., Junyaprasert, V.B., Chantasart, D., 2014. Development and characterization of lyophilized diazepam-loaded polymeric micelles. AAPS PharmSciTech 15, 52–64.

Sun, D.D., Lee, P.I., 2015. Haste makes waste: the interplay between dissolution and precipitation of supersaturating formulations. AAPS J. 17, 1317–1326.

Sun, H., Mumby, S.J., Maple, J.R., Hagler, A.T., 1994. An ab Initio CFF93 all-atom force field for polycarbonates. J. Am. Chem. Soc. 116, 2978–2987.

Ueda, K., Taylor, L.S., 2021. Partitioning of surfactant into drug-rich nanodroplets and its impact on drug thermodynamic activity and droplet size. J. Control. Release 330, 229–243.

Ueda, K., Higashi, K., Moribe, K., 2017. Direct NMR monitoring of phase separation behavior of highly supersaturated nifedipine solution stabilized with hypromellose derivatives. Mol. Pharm. 14, 2314–2322.

Van den Mooter, G., 2012. The use of amorphous solid dispersions: a formulation strategy to overcome poor solubility and dissolution rate. Drug Discov. Today Technol. 9, e79–e85.

Vasconcelos, T., Sarmento, B., Costa, P., 2007. Solid dispersions as strategy to improve oral bioavailability of poor water soluble drugs. Drug Discov. Today 12, 1068–1075.

Wang, X., Michoel, A., Van den Mooter, G., 2005. Solid state characteristics of ternary solid dispersions composed of PVP VA64, Myrj 52 and itraconazole. Int. J. Pharm. 303, 54–61.

Williams, H.D., Trevaskis, N.L., Charman, S.A., Shanker, R.M., Charman, W.N., Pouton, C.W., Porter, C.J.H., 2013. Strategies to address low drug solubility in discovery and development. Pharmacol. Rev. 65, 315–499.

Xie, T., Taylor, L.S., 2016. Dissolution performance of high drug loading celecoxib amorphous solid dispersions formulated with polymer combinations. Pharm. Res. 33, 739–750.

Yuan, X., Sperger, D., Munson, E.J., 2014. Investigating miscibility and molecular mobility of nifedipine-PVP amorphous solid dispersions using solid-state NMR spectroscopy. Mol. Pharm. 11, 329–337.

Zhang, W., Hate, S.S., Russell, D.J., Hou, H.H., Nagapudi, K., 2019. Impact of surfactant and surfactant-polymer interaction on desupersaturation of clotrimazole. J. Pharm. Sci. 108, 3262–3271.